MULTI-SCALE MAPPING AND ACCURACY ASSESSMENT OF LEAF AREA INDEX FOR VEGETATION STUDY IN SOUTHERN ILLINOIS

By

Kushendra Narayan Shah

B.S., Kathmandu University, 2008

A Thesis
Submitted in Partial Fulfillment of the Requirements for the
Master of Science Degree

Department of Geography and Environmental Resources
In the Graduate School
Southern Illinois University Carbondale
August 2013

THESIS APPROVAL

MULTI-SCALE MAPPING AND ACCURACY ASSESSMENT OF LEAF AREA INDEX FOR VEGETATION STUDY IN SOUTHERN ILLINOIS

By

Kushendra Narayan Shah

A Thesis Submitted in Partial

Fulfillment of the Requirements

for the Degree of

Masters of Science

in the field of Geography and Environmental Resources

Approved by:

Dr. Guangxing Wang, Chair

Dr. Tonny Oyana

Dr. Samuel Adu-Prah

Graduate School

Southern Illinois University Carbondale

May 20, 2013

AN ABSTRACT OF THE THESIS OF

Kushendra Shah, for the Master of Science degree in Geography and Environmental Resources, presented on May 20, 2013, at Southern Illinois University Carbondale.

TITLE: MULTI-SCALE MAPPING AND ACCURACY ASSESSMENT OF LEAF AREA INDEX FOR VEGATION STUDY IN SOUTHERN ILLINOIS

MAJOR PROFESSOR: Dr. Guangxing Wang

The increasing interest of modeling global carbon cycling during the past two decades has driven this research to map leaf area index (LAI) at multiple spatial resolutions by combining LAI field observations with various sensor images at local, regional, and global scale. This is due to its important role in process based models that are used to predict carbon sequestration of terrestrial ecosystems. Although a substantial research has been conducted, there are still many challenges in this area. One of the challenges is that various images with spatial resolutions varying from few meters to several hundred meters and even to 1 km have been used. However, a method that can be used to collect LAI field measurements and further conduct multiple spatial resolution mapping and accuracy assessment of LAI is not available. In this study, a pilot study in a complex landscape located in the Southern Illinois was carried out to map LAI by combining field observations and remotely sensed images. Multi-scale mapping and accuracy assessment of LAI using aerial photo, Landsat TM and MODIS images were explored by developing a multi-scale sampling design.

The results showed that the sampling design could be used to collect LAI observations to create LAI products at various spatial resolutions and further conduct accuracy assessment. It was also found that the TM derived LAI maps at the original and aggregated spatial resolutions successfully characterized the heterogeneous landscape and captured the spatial variability of LAI and were more accurate than those from the aerial photo and MODIS. The aerial photo derived models led to not only over- and under-estimation, but also pixilated maps of LAI. The MODIS derived LAI maps had an acceptable accuracy at various spatial resolutions and are applicable to mapping LAI at regional and global scale. Thus, this study overcame some of the significant gaps in this field.

ACKNOWLEDGMENTS

I would like to express my sincere gratitude to my adviser, Dr. Guangxing Wang for his remarkable assistance throughout this study. While working together, his invaluable guidance, support, and instructions helped me a lot. I would also like to thank my committee members: Dr. Tonny Oyana and Dr. Samuel Adu-Prah for their feedback and inputs. Indeed, they had provided noble ideas and approaches beyond my thesis work too. Moreover, my sincere thanks go to Mr. Santosh Rijal and Samir Shrestha for their rigorous work in data collection and without them it would be difficult for me to complete the field work. Last but not the least; I would like to thank my geography team mates and staff for their moral support and inspiration.

TABLE OF CONTENTS

LIST OF TABLES

TABLE

PAGE

LIST OF FIGURES

CHAPTER 1

INTRODUCTION

1.1 BACKGROUND

Combining remotely sensed imagery and ground truth data to study terrestrial vegetation and land cover changes has been practiced for several decades. Such studies help to develop climate models in terrestrial ecosystems at a regional and global scale (Chen 2005). Moreover, plant vegetation plays a vital role in the assimilation of carbon-dioxide (Turner et al. 2004) and sequestering carbon compounds from atmosphere. Quantifying the presence of vegetation cover in the terrestrial landscape often requires accurately mapping of above ground biomass. Multi-scale mapping in conjunction with biomass variables such as Leaf Area Index (LAI) has a great significance for future research and applications (Wulder et al. 2004). Such variables coupled with remote sensing helps to compute above ground biomass or vegetation cover by building empirical relationship between vegetation cover with spectral variables from remotely sensed images (Friedl et al. 1994; Zha et al. 2003; Gray and Song 2012). In doing so, among several vegetation variables, LAI as a primary variable is crucial for characterizing energy and mass exchange for modeling carbon change and phenology, evapo-transpiration, and estimating primary productivity of ecosystems at global scale (Spanner et.al. 1990; Turner et al. 2004; Valdez et al. 2012).

According to Chen & Black (1992), LAI is defined as the total one-sided leaf area per unit ground area. Its values range from 0 (bare ground) to over 10 (dense forest) and depending upon the plant types, canopy cover and vegetation structure. LAI is dimensionless. The higher the vegetation canopy density and biomass, the larger the values of LAI. LAI is responsible for exchange of water, carbon and other compounds that involve all process based models (Running et al. 1989; Chen 2013). At canopy level, the radiation portions of specific wavelengths are intercepted, absorbed and reflected by plant leaves, which can be determined by the amount of LAI. LAI data collected at landscape scales provides analysis of canopy architecture, light intercepted at canopy level and spectral reflectance of canopy structure and ground (Valdez et al. 2012). This reflectance of canopy will produce a remote sensing signal that depends on the amount of leaf presence and its architecture (Chen 2013). Thus, remotely sensed images provide the great potential to develop spatial explicit estimates of LAI.

Although the use of remotely sensed images provides a feasible measure for mapping LAI continuously over terrestrial landscapes, accurate estimation of LAI for a study area is a challenging task (Gray and Song, 2012). First of all, mapping LAI at landscape, regional and global scale requires collection of LAI ground observations and this is often money-consuming. Secondly, multiple spatial resolution images have been widely used to map LAI from a local scale to a regional and global scale. For example, Landsat Thematic Mapper ™ images with medium spatial resolution of 30 m x 30m have been employed to map LAI at local and national level whereas MODIS (moderate resolution imaging spectro-radiometer) images lead to lower spatial resolution LAI products at 250 m, 500 m and 1000 m. However, LAI observations are often collected at sample plots that have spatial resolutions from 1 m × 1 m to 30 m × 30 m. Thus, there is an inconsistency of spatial resolutions between the sample data and images, which leads to the difficulty of combining the sample data and remotely sensed images to create LAI maps. A typical example is how to combine the MODIS images at a spatial resolution of 1000 m × 1000 m with LAI measurements that are collected at sample plots of 10 m × 10 m. Moreover, the relationships of LAI observations with spectral variables from remotely sensed images vary depending on spatial resolutions and thus different algorithms may be needed for mapping LAI at multiple scales (Jonckheere et al. 2004; Chen 2013). In addition, there is no an effective method to assess the accuracy of LAI estimates at multiple scales.

This study focused on derivation of LAI estimates and accuracy assessment at multiple spatial resolutions by combining LAI observations from sample plots and various remotely sensed images including aerial photographs, Landsat TM images, and MODIS at the Southern Illinois. Furthermore, this study investigated and analyzed an efficient sampling design for collecting LAI measurements for mapping and validation of LAI at multiple spatial resolutions across a heterogeneous landscape in the Southern Illinois. Theoretically, this study attempted to overcome some of the gaps that currently exist in this field.

1.2 PROBLEM STATEMENT

With the advent of remote sensing technologies in late 20th century, land surface processes and global carbon modeling have been studied frequently. The primary goal of remote sensing is to continuously observe land surface conditions and processes at various scales (Huete et al. 2002). For carbon cycle modeling at local, regional and global scales, there has been a strong need to map spatial distributions and patterns of vegetation canopy across heterogeneous landscape. There is also a gap in the study of quantification and effective mapping of the spatial distributions and patterns of biomass or carbon that is driven by LAI (Wang et al. 2009). The inconsistency of spatial resolutions when remotely sensed images and LAI observations are used to map LAI largely impedes the development of models and algorithms that are used to combine remotely sensed images and LAI observations and ultimately affects the accuracy of maps. Moreover, it is important to apply multiple spatial resolution images to explore vegetation structures and patterns. For doing this, an effective sampling design to collect in situ LAI measurements at multiple spatial resolutions are required (Chen 2013).

Carbon mapping for heterogeneous landscapes like Southern Illinois where the vegetation is sporadically populated is itself challenging and tedious. Vegetation cover of Southern Illinois is comprised of forests, grass lands, and crop lands. The forested region represents hardwood lands dominated by oak-hickory species. Although debates have been still persisted to know if the forests are sinks or sources of carbon however, there is a significant need to identify whether the hardwood forests are carbon sinks or sources (Luyssaert et al. 2008; Pregitzer and Euskirchen 2004). For this research, a pressing need is to map spatial distribution of LAI and monitor its spatial variability in terms of vegetation structure for example, hardwood forests. Owing to the fragmented landscape of Southern Illinois, it is important to know the amount of vegetation condition that can be achieved by measuring Leaf Area Index parameter in Southern Illinois. Furthermore, no studies that deal with mapping LAI in Southern Illinois have been carried out. Thus, this research will certainly help provide information on these topics.

In addition, there is also a need to clarify if the accuracy of MODIS derived LAI maps are compatible with that of Landsat TM image derived LAI estimates. Landsat TM images have a spatial resolution of 30 × 30 m and usually can be used to map LAI at local and regional scales, while MODIS images have a range of spatial resolutions from 250 × 250 m to 1000 × 1000 m and are often applied to map LAI at regional and global scales. That means that the coarse spatial resolutions of MODIS do not allow for spatial details to be mapped as much as landsat TM (Cohen et al. 2003). On the other hand, the MODIS derived LAI maps may be problematic for their applications at the local scale. Because of larger pixel sizes in MODIS images, it is expected that smoothing of spatial variance of pixel values could result in lesser spectral sensitivity to LAI (Woodcock & Strahler 1987; Cohen et al. 2003). In an earlier investigation, Doraiswamy et al. (2004) found that MODIS images at 1-km resolution couldn't be able to specify crop LAI because the 1-km spatial resolution is a limiting factor in accurately retrieving crop-specific biophysical parameters at field and local scales. In order to address the accuracy of MODIS product, there is a strong need to assess the quality of MODIS derived LAI maps. In this study, the comparison of MODIS and Landsat TM derived LAI maps will provide the fundamental information on assessing its quality and the linkage from local LAI maps to regional and global LAI maps. Thus, this research will further clarify these issues.

1.3 STUDY OBJECTIVES

The purpose of this study was to develop an effective sampling design for collecting ground measurements of LAI at different spatial resolutions across the heterogeneous landscape of Southern Illinois. This design aimed at successfully combining field sample plot data with aerial photographs, Landsat TM images, and MODIS images and performing accuracy assessment at different spatial resolutions that vary from 1m x 1m to 30 m x 30 m, 90 m x 90 m, 250 m x 250 m, 500 m x 500 m, and 1000 m x 1000 m. Moreover, this research explored the correlations of LAI measurements with the used images and their various transformations and investigated the development of models that account for the relationships at multiple spatial resolutions. A best regression model was obtained for each spatial resolution. This study also analyzed the relationships of LAI spatial distributions with vegetation types including grass land, cropland, and forests, and thus provided estimates of LAI as a vital source of information in process based models that are used to clarify if the hardwood forests in this area are carbon sinks or sources. In addition, this study undertook a comparison of spatial details and accuracy of LAI maps derived by aerial photos, Landsat TM and MODIS in Southern Illinois and thus clarified whether MODIS derived LAI maps can be used to provide LAI information for vegetation carbon cycle modeling at local and regional scales.

1.4 RESEARCH QUESTIONS

This study tested the following hypotheses: i) the spectral variables from Landsat TM and MODIS images are significantly correlated with LAI; and ii) MODIS derived LAI maps have significantly lower accuracy and less details than the Landsat TM derived LAI maps. Moreover, this study tried to answer following questions:

1) What sampling design method is effective to collect measurements of LAI for the heterogeneous landscape in Southern Illinois so that the obtained LAI observations can be used to map LAI and validate the accuracy of the maps at different spatial resolutions?
2) How does LAI vary over space depending on different vegetation types and canopy structures, including forests, crop lands and grass lands?
3) Does a MODIS derived LAI map have significantly lower accuracy and less details than a Landsat TM derived LAI map?

CHAPTER 2

REVIEW OF LITERATURE

2.1 BACKGROUND

Various studies have been done regarding the application of remote sensing to vegetation carbon modeling at various spatial and temporal scales. However, there are still some great challenges in generating continuous time series of vegetation products from multiple sensor instruments (Ganguly et al. 2008). There are also global concerns regarding climate change and how carbon cycling affects climate change. Some studies on LAI coupled with remote sensing technologies provide an insight of dynamic changes in productivity and climate impacts on vegetation ecosystem (Zheng and Moskal 2009). The abundance of vegetation cover on terrestrial surface plays an important role on mitigation of carbon concentration in atmosphere. Vegetation types, canopy structures, and plant physical characteristics are the important factors taken into consideration for modeling biophysical variables in terrestrial surface. Especially, LAI is useful to study plant photosynthesis, growth and energy exchange between the surface of the earth and atmosphere. LAI is considered as an important variable in biomass study (Watson 1947; Chen and Black 1992) as the most important biophysical parameter and critical indicator of terrestrial ecosystems because of its significant role in photosynthesis, transpiration, carbon and nutrient cycling (Chen and Cihlar 1996; Breda 2003).

2.2 IMPORTANCE OF LAI AND ROLE OF REMOTE SENSING

Chen et al. (1997) highlighted the importance of LAI estimates as eco-physiological measure and remote sensing measure to understand the photosynthetic and transpiration activity as well as its spectral reflectance within canopy. Such reflectance is largely influenced by the optical properties of leaf and surrounding, topography, spatial resolution and look angle of sensors (Wulder et al. 2004; Chen 2013). Given the higher density of canopy structure, more absorption at blue and red wavelengths and more reflectance at green and near infrared of solar radiation occur and less energy can be transmitted to ground surface (Gobron et al. 1997; Zheng and Moskal 2009). Also it is noted that healthy plant leaves absorb most visible solar radiation and scatter non visible component. Various remote sensing technologies and sensors help in mapping LAI by developing a suitable relationship between spectral response and magnitude of LAI (Wulder et al. 2004). On developing the relationship, recent years LAI research is profoundly geared towards practical and process based modeling (Running and Gower 1991; Running and Hunt 1993). The process based models simulate biophysical processes and carbon sinks of plants by using LAI as a primary variable (Breda 2003). However, the process based models used for modeling vegetation carbon dynamics do not account for spatial variability of LAI and other parameters and variables. Remote sensing provides a powerful mechanism for the spatial estimation of LAI. The use of remote sensing provides the potential to create LAI products of vegetative growth conditions at various spatial resolutions (Chen 2005). The combination of the process based models and remotely sensed image derived LAI can lead to maps that account for spatial distribution of vegetation carbon and can be used to improve decision-making on carbon science management (Running and Gower 1991; Running and Hunt 1993; Wang et al. 2009).

2.3 TECHNIQUES AND MEASUREMENT OF LAI

Direct and indirect estimations are commonly two ways to quantify LAI of vegetation canopy in terrestrial landscape. The direct estimation known as destructive sampling method is based on the field based measurement and done by defoliation of leaf or litter fall collection, or point contact sampling (Chen et al. 1997). It basically involves collection and removal of green leaves or some representative trees from a sample plot (Zeng and Moskal 2009). This is accurate but labor intensive, time consuming and costly (Peduzzi et al. 2012) and hence adopted less frequently these days. One of the examples is the estimation of LAI using destructive sampling to obtain ground truth data in Yosemite National Park (Schiffman et al. 2008). Chen et al. (1997) also mentioned the direct destructive sampling method used in agricultural practice. However, sampling associated with this technique is less significant to evergreen forests because of absence of needle fall (Chen et al. 1997; Jonckheere et al. 2004). Also, it is difficult to directly perform LAI measurement over large spatial extents (Zheng and Moskal, 2009).

Non contact method of measurement based on light below and above the canopy (Eklundh et al. 2001) is more efficient and pragmatic compared to the aforementioned direct method. This indirect method holds a great promise because of its potential to obtain quick and low-cost measurements over large areas (Chen et al. 1997). This type of measurements can be collected for any heterogeneous surface of terrestrial ecosystems using airborne and satellite systems. Indirect estimation behind LAI measurement is guided basically by Radiative transfer model and commercial canopy analyzers.

The mechanism of radiative transfer model is based on measuring transmission of radiation through the canopy and is termed as radiative transfer theory (Ross 1981). This process is based on gap fraction that is guided by amount of light not penetrating to the understory from the canopy (Zeng and Moskel 2009). The gap fraction helps to measure amount of light penetration and gaps in the canopy (Zeng and Moskel 2009) and is determined by leaf distribution and arrangement at canopy level (Campbell 1986). The radiative transfer model can be written as:

$$LAI = \ln(P(\theta))\cos(\theta) / G(\theta) \quad (1)$$

Where P(θ) is the gap fraction, G(θ) represents foliage projected to the leaf angle distribution. According to Breda (2003), radiative measurement method is based on Beer-lambert equation that involves measuring incident radiation I_0 (Yang et al. 1993; Zheng and Moskal 2009). The below-canopy radiation is measured as:

$$I = I_0 e^{-k \times LAI} \quad (2)$$

Where *k* is the extinction coefficient and is function of leaf angle distribution. Previous studies show various ways of measuring LAI of canopy that is influenced by canopy distribution pattern. Chen et al. (1997) formulated effective LAI for in situ measurement that is used for nonrandom dispersion of canopy is given as:

$$L_e = \Omega L \quad (3)$$

Where L_e represents the effective plant area index, L is the actual biomass area, and **Ω** is the clumping index and its value attains a unit when biomass is randomly distributed. Similarly, in other study of random distribution pattern by Chen et al. (1997), canopy gap fraction is derived to obtain “effective” LAI estimate using radiative transfer model. The model expressed as:

$$L = (1-\alpha)L_e \quad (4)$$

Where α is the critical component in optical LAI measurement, L is the actual LAI and L_e represents the effective LAI.

Moreover, the study of LAI has been widely conducted by plant canopy analyzers. The study by Breda (2003) mentioned four types of plant canopy analyzers that are used on estimating LAI by measuring light transmitted through canopy. Instrument such as Accupar (Decagon devices, USA) and Sunscan (Delta-T Devices, UK) are used to measure the incident photosynthetically active radiation (PAR) and transmitted PAR above canopy and below canopy. Similarly, other two kinds of instrument like LAI-2000 (Li-Cor, Nebraska) and DEMON (CSIRO, Australia) are used for above canopy with fixed below canopy in range of 320 – 490 nm and 430 nm, respectively.

However, there is no clear understanding as to which approach produces best results for a given land cover type. Qi et al. (2000) suggested two common approaches which are similar to the notion developed by Chen et al (1997) to estimate LAI using remote sensing imagery: (1) vegetation index approach and (2) modeling approach. Vegetation index approach is associated with spectral transformation of two or more bands in order to understand vegetation properties such as normalized difference vegetation index (NDVI) (Rouse et al. 1974; Qi et al. 2000; Huete et al. 1997). Modeling approach is based on determination of spatio-temporal dynamics of vegetation variable such as LAI, across the wide range of areas by establishing empirical relationship (Chen and cihlar 1996; Myneni et al. 1997; Hassan and Bourque 2010; A.Vina et al. 2011).

Several algorithms have been derived by using multiple band combinations from spectral data and deriving vegetation indices (Vina et al. 2011). Since the portion of LAI is composed of green leaf area as photosynthetically functional component (Vina et al. 2011), the most common vegetation index to measure the greenness is NDVI that is based on red and near-infrared reflectance: $NDVI = (\rho_{NIR} - \rho_{\mathrm{Red}})/(\rho_{NIR} + \rho_{\mathrm{Red}})$, where ρ is the spectral reflectance (Rouse et al.

1974; Heute et al 2002). Given the high reflectance of RED and low in NIR, a small value can be obtained for NDVI (Turner et al. 1999). Plant foliage will have relatively low reflectance of red energy when there is high absorption of red wavelength (Turner et al. 1999). Conversely, dense vegetation canopy will have high reflectance in near infrared band, which leads to greater NDVI value. The reflectance and absorption of spectral data is guided by leaf optical properties which allows optical remote sensor to capture detailed information on photosynthetically active vegetation canopy structure (Zheng & Moskal 2009) and will help to understand energy exchange and carbon sequestration.

NDVI is affected by both canopy structure of plant and source-sensor geometry (Goetz 1997). Though NDVI is commonly used for global long-term vegetation monitoring, generally its relationship with LAI can be established on specific site, time and biome (Sellers et al. 1996). Therefore, it is important to analyze the relationship between LAI measured in the field and NDVI derived from Landsat TM images to generate LAI maps (Xavier and Vettorazzi 2004). Compared to other spectral variables, NDVI is often better correlated with LAI. In the recent study of Hassan and Bourque (2010) in Boreal Forest region of Northern Alberta, the results showed relatively strong linear correlation between LAI and vegetation index.

Huete et al. (1997) compared the capability of vegetation index products derived from MODIS images and found that NDVI is high dependent on red band in the forested region rather than the Soil adjusted Vegetation Index (SAVI). Huete et al. (2002) suggested high match between the values obtained from airborne and canopy reflectance with MODIS images. There is indeed a need to enhance the understanding of the correlations between LAI and various vegetation indices from satellite data from fine spatial resolutions to coarser ones.

Chen et al. (1997) gave an overview of estimating LAI for boreal forests, including theory, techniques and measurements. Zheng et al. (2009) summarized theories, methods and sensors for mapping LAI using remote sensing methods. They concluded that Landsat TM images have been widely used to map LAI of vegetation canopy (Cohen et al. 2003; Chen and Black 1992; Chen and Cihlar 1996; Xavier and Vettorazzi 2004). For example, Eklundh et al. (2001) investigated the relationships between Landsat ETM+ data and LAI in a boreal conifer forest. In the similar research by Cohen et al. (2003), an increasing correlation was obtained between reflectance and LAI data with increasing pixel size of MODIS imagery and they clarified the similarities and distinction between LAI estimates from MODIS and Landsat ETM plus images. Chen and Black (1992) mapped LAI of boreal conifer forests using Landsat TM images. Turner et al. (1999) investigated the relationship between LAI and Landsat TM spectral vegetation indices across three temperate zone sites. However, the methods to map LAI using remote sensing technologies greatly vary depending on spatial resolutions of images and the sizes of study areas.

Zha et al. (2003) conducted a spectral reflectance-based approach in western China and quantified percentage of grassland cover from Landsat TM imagery. They found significant statistical relationship between grass cover and NDVI with a small sample size. When a study area is large, such as the whole US or the earth surface, finer or medium spatial resolution images often lead to huge amounts of data and difficulties of calculation. Thus, coarser spatial resolution images such as MODIS are recommended. Chen et al. (2002) derived Canada-wide coarse-resolution LAI maps using satellite imagery and ground measurements. MODIS and AVHRR (Advanced Very High Resolution Radiometer) images at coarser spatial resolutions such as 1 km × 1 km have been widely used to map vegetation index and LAI at regional and global scales. However, the MODIS products that render the coarse-resolution images at a large scale require integrated approach to validate them based on the field measurements because LAI measurements are often collected at finer spatial resolution such as 30 m × 30 m (Cohen et al. 2003). In previous study by Spanner et al. (1990), TM images are sensitive to small scale variations in canopy closure, understory vegetation and background reflectance due to fine spatial resolution. On the other hand, finer spatial resolution images can record much complexity of land surface feature, while MODIS images lack of this type of spatial detail due to coarser spatial resolution (Cohen et al. 2003). It is important for regular and ongoing assessment of quality of remotely sensed image products at regional and global scale. But, the methods for the quality assessment are still lacking.

2.4 LAI ESTIMATION

Regression modeling is the most common method to estimate and map forest biomass characteristics (Jensen and Hardin 2005) and has been widely used for modeling the relationship between spectral data and LAI (Chen and Cihar 1996; Turner et al. 1999; Cohen et al. 2003). With the regression based approach, spectral values of remotely sensed data are paired with in situ LAI measurements (Fernandes et al. 2005). This is especially true when finer or medium resolution images are used. The performance of the method varies greatly depending on the correlation of LAI with spectral variables (Turner et al. 1999; Yang et al. 2006, 2007). The regression models often help to identify the strength of correlation between ground data with image bands. Xavier & Vettorazzi (2004) established the relationship between LAI with NDVI derived from Landsat TM images to obtain LAI map. They concluded that 72 percent of LAI variance could be explained by NDVI. In a similar study by Yang et al. (2007), regression model was developed between LAI of winter wheat and vegetation indices. They found that 70 percent variation of LAI was explained by the spectral variables from TM images. Zarate-Valdex et al. (2012) found a high correlation of LAI derived from hemispherical photography with MASTER Vegetation index. Multivariate stepwise regression is often used to select important predictor variables. Cohen et al. (2003) did OLS (Ordinary Least Square) and RMA (Reduced Major Axis) regression in multiple SVI to investigate the relationship between ETM+ and MODIS images. Hassan and Bourque (2010) used data fusion technique to establish linear correlation between LAI and EVI (Enhanced Vegetation Index). Similarly, Huang et al. (2006) used OLS regression model to generate a 30 m resolution LAI map for a 900 sq.km study area. But, regression modeling often leads to overestimation and underestimation of LAI (Ganguly et al. 2008).

Wang et al. (2009) proposed an image based co-simulation to map forest carbon stock and this method can also be used to map LAI by combining sample plot data and remotely sensed images. The shortcoming of this method is its complexity and hard to apply. Another kind of methods is nonparametric, such as K-Nearest Neighbors that examines each pixel to be estimated and identifies k-nearest training samples measured in multispectral space and then calculates and assigns a weighted average to the estimated pixel. Regardless of spatial resolutions and interpolation methods, the important principle to map LAI is that the spatial resolutions of plot data must be consistent with those of remotely sensed images (Wang et al. 2001 and 2009). Because of lack of field data at coarser spatial resolutions, the MODIS image derived LAI products are not often based on in situ measurements of LAI and currently there is also no effective way to valid the MODIS LAI products.

Various remotely sensed images from high resolution aerial photographs to medium resolution Landsat TM images and coarse resolution images such as MODIS have been widely used for mapping LAI. High spatial resolution images such as aerial images and Ikonos and Geo-

Eye images can provide the details of vegetation canopy structures and be often used as reference maps to assess medium and coarse resolution products (Wulder et al. 2004). This type of LAI maps at higher resolution can be used to enhance the understanding of above ground biomass at local scale. Yang et al. (2006) developed medium resolution LAI products to investigate spatial distribution and dynamics of land cover types. Landsat derived LAI maps provide more detailed information of LAI compared to MODIS derived LAI products and thus can be used as reference. However, an algorithm is required on how to validate the coarser LAI products using finer resolution maps because of different resolutions (Yang et al. 2006). Chen et al. (2002) mentioned that validation of LAI products from coarse resolution is challenging task due to limited collection of ground plot data. Usually, coarser resolution images like MODIS are employed to map LAI of large biomes at regional and global level (Cohen et al. 2006). The MODIS derived LAI products would help to understand the global dynamics of carbon cycling (Cohen et al. 2003). On the other hand, unlike Landsat TM images that have coarser temporal resolution, high temporal resolution MODIS images provide information in a timely basis (Schiffman et al. 2008). But, in terms of accuracy assessment, medium resolution image derived LAI maps are often more accurate (Chen et al. 2002). Therefore, there is a tradeoff between spatial and temporal resolution (Gray and Song 2012).

2.5 ACCURACY ASSESSMENT of LAI MAPS

The accuracy assessment of LAI maps can be quantified using root mean square error (RMSE) or Pearson product moment correlation coefficient between the estimated and observed LAI values (Wang et al. 2005, 2009; Wang and Gertner 2013). The focus is often put on the acquisition and use of sample plot data. There are three widely used methods (Congalton 1991;

Congalton and Green 2009). First of all, sometimes one uses a portion of a set of sample plots for model development and the rest for validation of obtained models. This method is limited because the sample plots used for accuracy assessment are not independent from those used for developing models. Secondly, cross-validation is another widely used method for accuracy assessment. In this method, each time one kicks out one sample plot and uses it as reference and then applies all the plots left to develop models. The obtained model is used to calculate an estimate for the plot that is removed and its square difference between the estimated and observed value is calculated. This process is repeated until the square differences for all the sample plots are obtained. This method leads to a RMSE and greatly saves time and money for collection of ground truth data, but implies a great load of computation. The best way for accuracy assessment is the acquisition and use of independent sample plots. However, this method is time and money consuming. Additionally, Wang and Gertner (2013) suggested the use of spatial uncertainty and error budget in which various sources of errors are identified and quantified and linked with the output uncertainties and the uncertainties of estimates are then partitioned into the input components of errors.

In addition to selection of methods, we are facing several other challenges for the accuracy assessment of LAI maps. First of all, the inconsistency of spatial resolutions for the sample plot data and used remotely sensed images often leads to difficulties of accuracy assessment (Wang and Gertner 2013). A typical example is that MODIS images produce 1 km ×1 km LAI products while the sample plot data are often collected at spatial resolutions that are much finer. Secondly, how to simultaneously assess the quality of LAI maps at multiple spatial resolutions is another great challenge and so far there are no studies that have been reported in this area (Wang and Gertner 2013). This obviously needs a multi-scale sampling design. This is one goal of this study.

Many studies reported that the LAI values derived from MODIS coarse-resolution images usually have lower accuracy than those from fine-resolution images (Chen et al. 2002; Yang et al. 2007). Busetto et al. (2007) combined medium and coarse spatial resolution images to estimate sub-pixel NDVI. Their result showed higher correlation and lower RMSE between MODIS and TM NDVI. Therefore, assessing the accuracy of LAI map is driven by the validation of using LAI estimates. There has been a significant error on coarse resolution MODIS products. This is especially true on estimation of LAI for forested biomes and LAI is often over-estimated compared to in situ observations (Kauwe et al. 2011). Therefore, accurate validation of using representative samples should be considered for assessing the quality of LAI maps. It is given by the confidence errors of prediction of the regression transfer function (Fernandes et al. 2005). Moreover, likely noticeable error considerably occurs due to sampling and measuring of LAI, algorithms, geometric correction and atmospheric correction and calibration of remotely sensed images, etc. (Fernandes et al. 2003). If there are no measurement errors, the model is a true representation of the ground characteristics and the estimates from it should be highly correlated with the ground truth (Wang et al. 2001).

CHAPTER 3

MATERIALS AND METHODOLOGY

3.1 STUDY AREA

The study area is located at Southern Illinois, which extends from southern part of Jackson County to northern part of Union county. It is joined with the Giant City State Park in the east and Shawnee National Forest in Northwest. This study area has a center at X-coordinate of 301380 m and Y-coordinate of 4165140 m under NAD 1983 Universal Transverse Mercator (UTM) 16N, and covers a total of 25 sq.km (Figure 1). The climatic pattern is continental, generally with hot summers and cold winters (Hosner and Minckler 1963). The average temperature ranges from a high of 30.6^0 C degrees to a low of 2.2^0 C degrees (http://www.netstate.com/states/geography/ il_geography.htm). Average precipitation is 29 cm in winter and 31 cm in summer (Illinois State Water Survey). The elevation ranges from 91 m to 325 m above sea level. The major soil types include *Alfisols, Entisols, Inceptisols, Mollisols* and *Ultisols* (Thompson 2004). The land use and land cover types include forests, shrubs, grasslands, and croplands. The land cover categories of Jackson County comprise agricultural land (91736 ha), rural grassland (31134 ha), forested land (37103 ha), wetland (16610 ha), and urban built-up land (5443 ha) (Land cover of Illinois Statistical Summary 1999-2000).

3.2 VEGETATION COVER TYPES

The study area consists of private, state, and federally owned land located in the vicinity of Shawnee National Forest and Interior Highlands of Ozark. The vegetation cover types include crops, shrubs, and forests. Common agricultural crops in this area are corn, soybean, and fruits.

The understory vegetation mainly consists of vascular plant communities like mosses and fern. The top canopy vegetation comprises of shrubs with native and invasive species such as honeysuckle (*Lonicera maackii*), Autumn olive (*Elaeagnus umbellate*), Common Reed (*Phragmites australis*), Nepalese browntop (*Microstegium vimineum*), Japanese knowtweed (*Polygonum* cuspidatum), Sawtooth oak (*Quercus acutissima*), etc.

The forested lands are dominated by species of Oaks and Hickories (Braun 1950). Because of the un-dissected till plain of southern Illinois, the oak- hickory association has also been influenced by the local soil type (Braun 1950). About ninety-eight percent of Illinois forests are composed of hardwood species (Illinois Department of Natural Resources 2008). The mixed forested lands in the study area are overwhelmingly dominated by deciduous hard wood species across the landscape (Fralish 2003) where most of the original stands of oak-hickory have been cleared and fragmented for agriculture purpose (Yates et al. 2003; Pande et al. 2006). Among the hard wood species, 43 percent are composed of white and red (Quercus rubra) oak (Illinois Department of Natural Resources 2008). Oak-hickory stands are the most common community that constitutes about 65% of the forested lands (USDA Forest Service 2009). The species are *Acer saccharum, Asimina triloba, Staphylea trifolia, Asplenium platyneuron, Botrychium dissectum, Fagus grandifolia* (Illinois Department of Natural Resources 2008).

A sampling design to collect LAI field observations was conducted in the summer of 2012. The sample consists of 175 plots (Figure 1). The sampling design method and data collection were described in the section of methods.

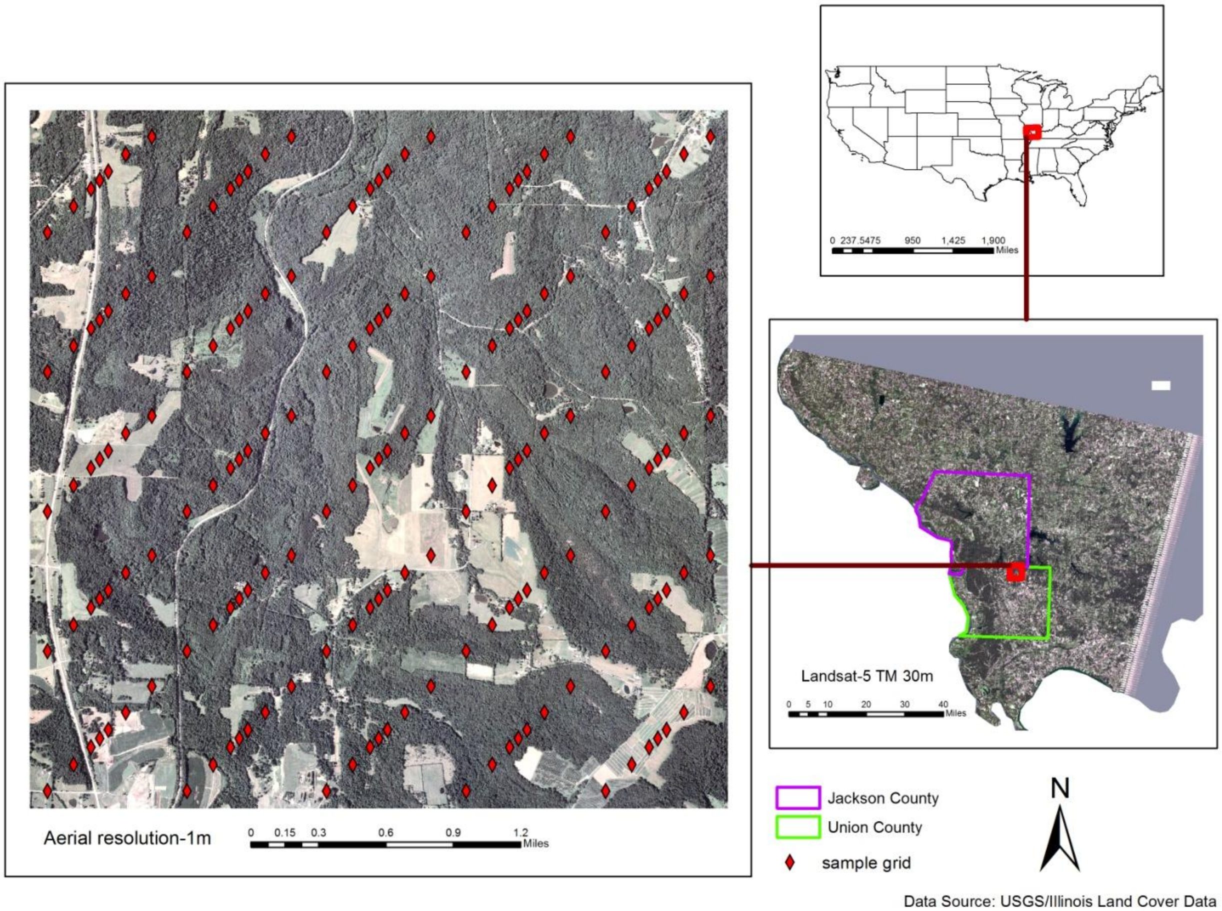

Figure 1: The study area illustrates the heterogeneous landscape of Southern Illinois. The red mark shows sampling grid in Jackson and Union county.

3.3 DATA SETS

3.3.1 HIGH RESOLUTION IMAGES: AERIAL PHOTOGRAPH

A high spatial resolution aerial photograph of Southern Illinois dated back on 2007 was obtained from Illinois Spatial Data Center (Figure 1). This aerial photograph had a spatial resolution of 1m and consisted of visible bands, i.e., red, green, and blue. This photo was geo-referenced with NAD 83 UTM Zone 16 coordinate system. Each visible band was extracted to form band ratios. Pixels values from all the bands and their ratios were extracted to match with the sampling plots. The aerial photograph did not match the sample plot data in terms of acquisition time very well. However, because there were no clearing cuttings and urbanizations that took place in this area, it can be assumed that the inconsistency of time would not lead to great uncertainty of the results and thus not affect the conclusions made from this study.

3.3.2 MEDIUM RESOLUTION IMAGES: LANDSAT TM IMAGERY

Landsat TM images have an appropriate spatial resolution of 30 m and thus provide the potential to create LAI vegetation products for the Southern Illinois. Landsat TM images with 16 days temporal resolution allow discriminating growth of vegetation and dynamics of land cover types such as grasses, shrubs, and forests. Given the high temporal period, it is better to obtain TM data for vegetation cover during summer because vegetation cover is particularly enhanced by plant growth that results in high biomass and PAR values (Chen et al. 2010). TM images consist of blue band 1 : 0.45 - 0.515 µm, green band 2: 0.525 - 0.605 µm, red band 3: 0.630 - 0.690 µm, near infrared (NIR) band 4: 0.74 - 0.90 µm, middle infrared (MIR) band 5: 1.55 - 1.75 µm and band 7: 2.08-2.35 µm. The appropriate spatial, spectral, and temporal resolution from TM images provides useful information to map LAI for southern Illinois (Schiffman et al. 2008; Zheng and Moskel 2009).

The entire study area was covered by a Landsat 5 TM scene: **Path 23** and **Row 34**. Although it was attempted to acquire the Landsat TM image of 2011 and 2012, due to high cloud cover, none of the TM scenes for the entire summers could be acquired for the study area.

Finally, a cloud free TM image was acquired on August 17, 2010 to conduct estimation of LAI (Figure 2). This image was radiometrically corrected and digital numbers were converted to reflectance values using Emperical Line Calibration (ELC) in order to reduce the effects associated with atmospheric interference including clouds and noise (Jensen 2005). The subset TM image was geometrically corrected with acceptable accuracy and was geo-referenced to the aerial photo that had NAD1983 UTM 16N coordinate system. The root mean square (RMS) error obtained was less than 0.5 pixel (<15m). After the pre-processing of TM image, the converted reflectance values were extracted from each band using the coordinates of LAI sample plots. In addition, the TM image data at the spatial resolution of 30 m × 30 m were aggregated to spatial resolutions 90 m × 90 m, 250 m × 250 m, 500 m × 500 m, and 1000 m × 1000 m using a window averaging method.

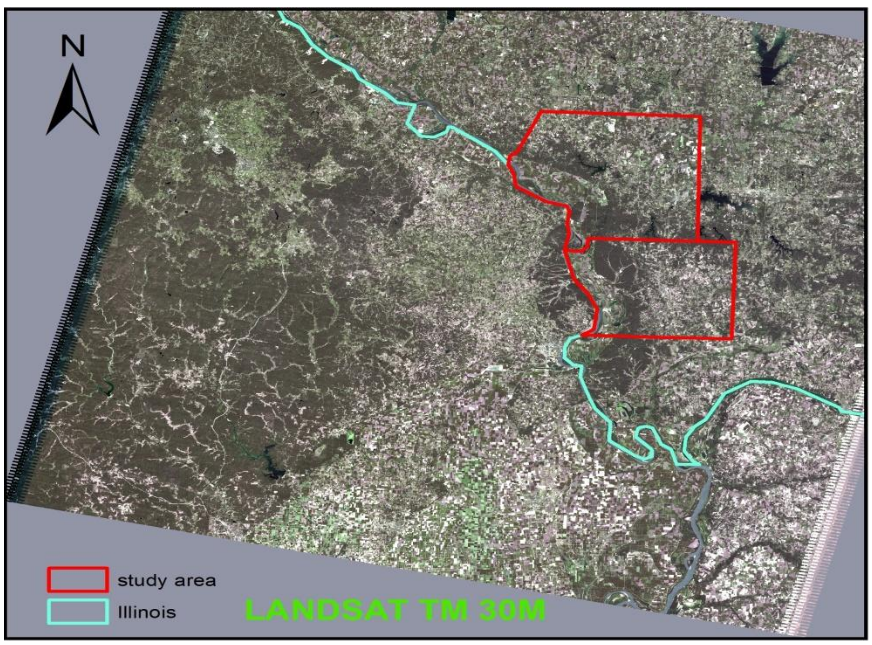

Figure 2: Landsat TM 5 image of Southern Illinois acquired on August 17, 2010. Upper red boundary shows Jackson County and lower red boundary shows Union County.

3.3.3 COARSE RESOLUTION IMAGES: MODIS IMAGERY

MODIS, aboard in the Aqua (EOS PM) and Terra (EOS AM) satellite platforms, provides the robust and pragmatic measures for monitoring dynamics of terrestrial vegetation ecosystems at regional and global scale. With its high temporal resolution (1 to 2 days), it monitors biophysical activity and vegetation parameter like LAI in routinely manner and performs time-series analysis. This remote instrument provides data of land, atmosphere, cryosphere, and ocean in 36 spectral bands. These bands have spatial resolution of 250 m (bands 1 - 2), 500 m (bands 3 - 7) and 1km (bands 8 - 36). Given the time of the day, on which the field data was collected, MODIS aboard Aqua platform dated on August 17, 2012 was downloaded in HDF format to produce multiple LAI products of different resolutions. This Aqua platform aboard MODIS sensor passes from south to north over the equator in the afternoon which was corresponded with the time of the day for data collection. The grided image of tile units (h-10, v-5) that centered the study area showed spatial and temporal variation of LAI at 16 days composite. The LAI products of different spatial and temporal resolution obtained (Figure 3) are given as:

- MYD13Q1: 16-day 250m VI
- MYD13A1: 16-day 500m VI
- MYD13A2: 16-day 1000m VI
- MOD 15A2: 8-day 1000m LAI

The vegetation products of each resolution obtained from the tile units that are in sinusoidal grid projection were re-projected to convert into UTM coordinate system using MODIS Re-projection Tool (MRT). This made a direct comparison and avoided large-scale distortions in the native projection system (Kauwe et al. 2011).The individual band layers were subset and layers stacked. The output file for each composite imagery contained red (620 - 670 nm), blue (459 - 479 nm), near infrared (841 - 876 nm), and middle infrared (1230 – 1250 nm, 1628 – 1652 nm, 2105 - 2155 nm). Similarly it also consisted of NDVI and enhanced vegetation index (EVI) images with parameters of view zenith, solar zenith, and relative azimuthal angles. The purposes of acquiring and using the MODIS images included (1) conducting an analysis of LAI estimates derived from each MODIS resolution image and (2) comparing the MODIS results with the TM derived LAI maps.

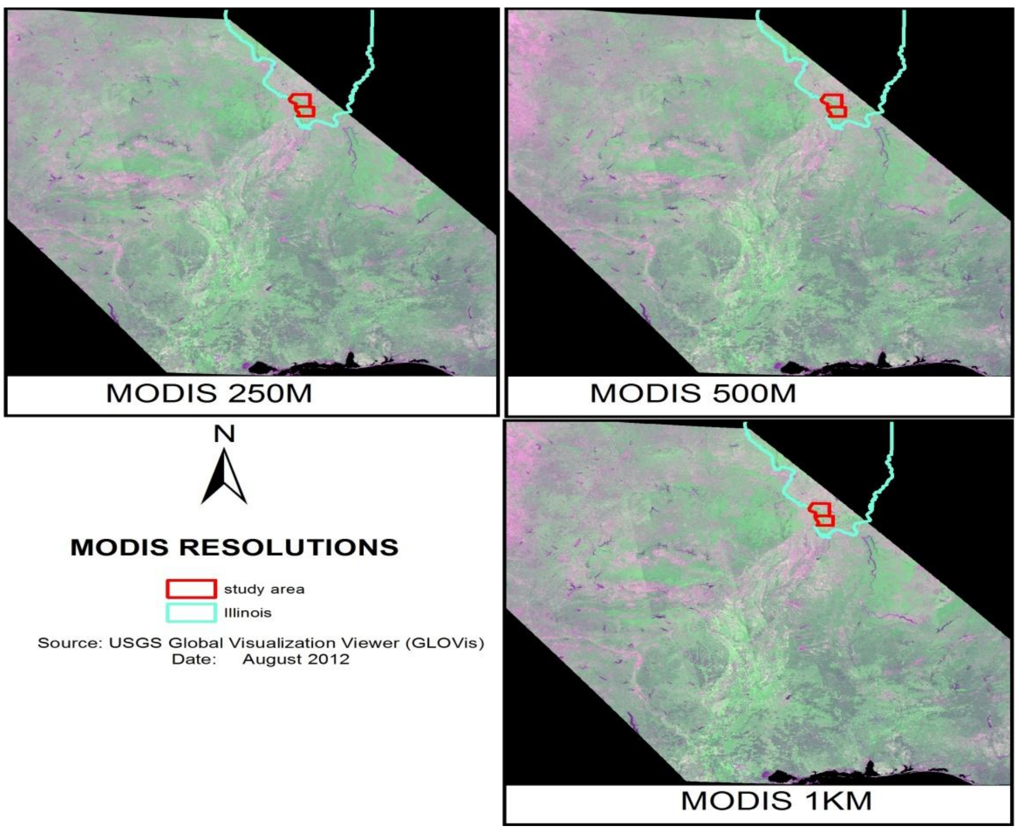

Figure 3: MODIS images of Southern Illinois acquired on August 17, 2012.

3.4 FLOW CHART OF THE METHODOLOGY

Figure 4 shows the flow chart of the methodology that consisted of study area, image acquisition, sampling design and collection of LAI in situ measurements, regression model at multiple spatial resolution, and accuracy assessment.

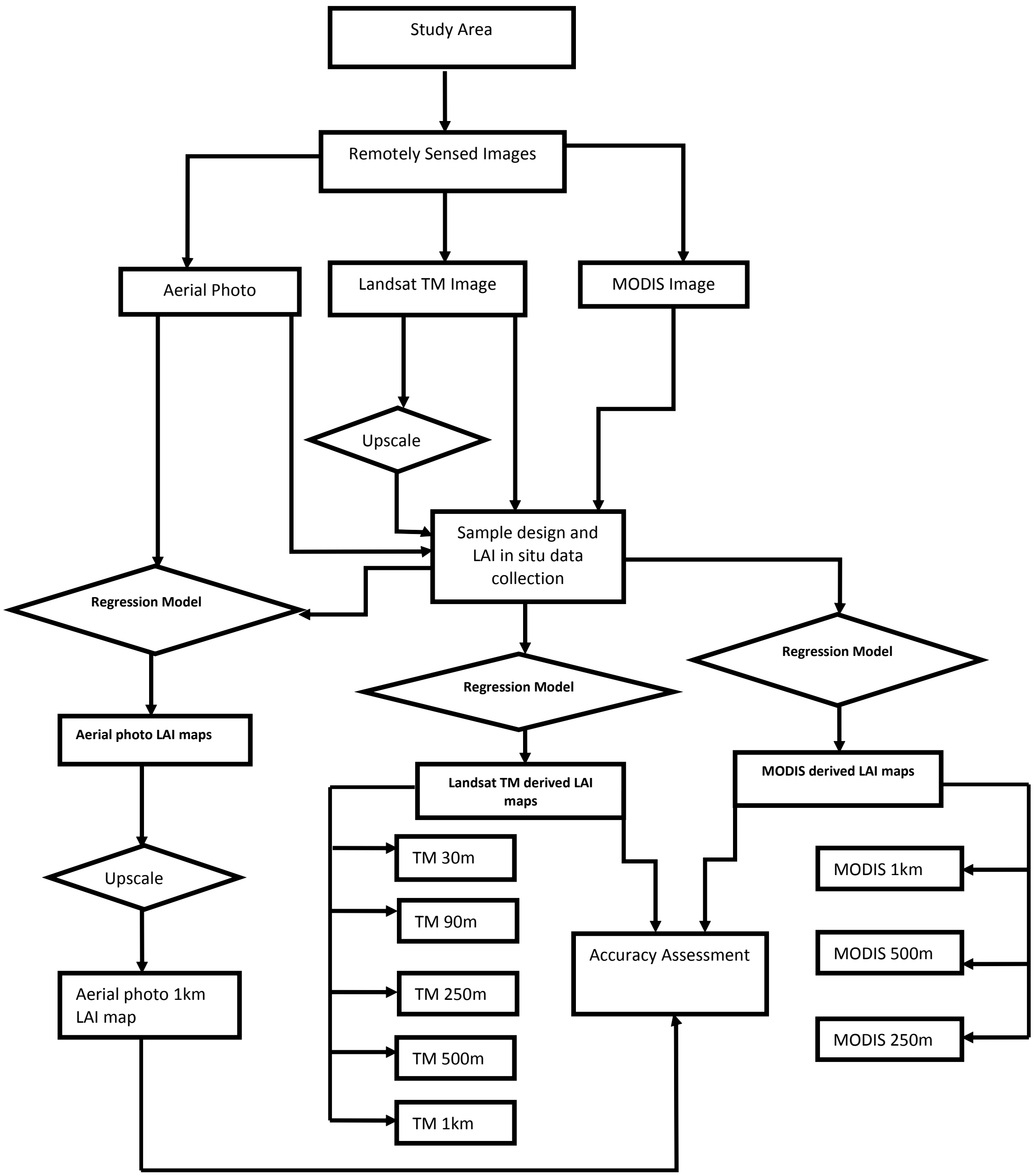

Figure 4: Flow chart of the methodology.

3.5 SAMPLING DESIGN AND LAI FIELD MEASUREMENTS

A systematic sampling for effective collection of measurements of LAI was designed so as to cover the study area (Figure 1) at varied grids and spatial resolutions including 1m, 30 m, 250 m, 500 m, and 1000 m. This design undertook series of steps and provided a potential to match the obtained field LAI measurements with remotely sensed images at multiple spatial resolutions for mapping LAI and conducting corresponding accuracy assessments of LAI maps.

A total of 25 blocks having 1 sq.km each was designed to stratify the landscape to collect LAI field measurements on different vegetation types. A systematic sampling design was conducted to generate a total of 175 sample plots. Each of the blocks corresponded to the pixel size of MODIS 1 km x 1 km spatial resolution images. Each of the blocks contained 7 sampling plots of 30 m x 30 m. The sampling plots were allocated along the diagonal line of the block to cover most of the portion inside the block so as to create a good representation of sample measurements. Each block was further divided into sub-blocks of sizes 500 m x 500 m, 250 m x 250 m, and 30 m x 30m in which a sample plot of 30 m x 30m that matched pixel size of Landsat TM images was centered. The blocks of 1000 m x 1000 m, 500 m x 500 m, and 250 m x 250 m matched three spatial resolutions of MODIS images. In each 250 m sub-block, 3 sample plots were allocated at the center and one at the half way of the diagonal line each side from the center to form systematic sample plots. In the same way, a total of 5 sample plots were allocated within each of the 500 m x 500 m sub-blocks and eventually, a total of 7 sample plots within each of the 1000 m x 1000 m blocks (Figure 5). Within each sample plot of 30 m x 30m, 5 transect lines were laid out to get 5 LAI field measurements in an interval of 6 m (Figure 6). A AccuPAR Lp-80 plant ceptometer (Decagon Devices, Inc., Pullman, WA, USA) was used to obtain LAI values in perpendicular to the transect line. The measurements had a spatial resolution of 1 m transect line that matched the pixel size of the used aerial photo. Considering each biomass vegetation canopy in transect line, the LAI value was recorded in variable landscape. Lastly, the coefficient of variation was calculated based on the number of observations and samples to be collected.

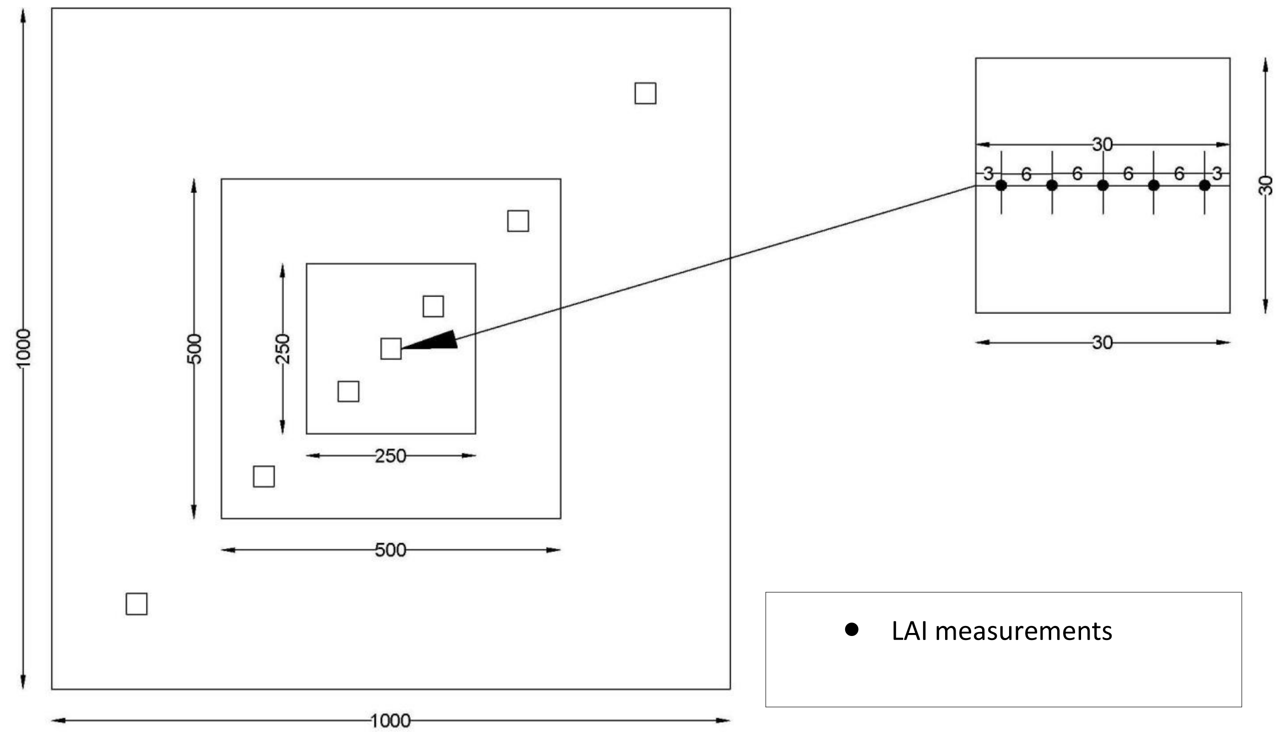

Figure 5: Allocation of sample plots along a transect line within each 1 km × 1 km block and collection of LAI measurements within each of 30 m × 30 m sample plot.

(a)

(b)

(C)

Figure 6: (a) A sample plot used to collect grassland LAI measurements taken in Southern Illinois; (b) Apple orchard standing in the transect line; and (c) A sample plot in crop land.

3.5.1 INDIRECT MEASUREMENT OF LAI

Field sampling was conducted at post morning and afternoon time periods in June of 2012. Prior to the ground measurement, a hand-held GPS device was used to precisely geo-locate (accuracy <5m) the designated area for obtaining ground-truth data through specified coordinates of the plot center. Once a sampling plot was fixed, the transect line was designated in every 6-m interval distance. The AccuPAR Lp-80 plant Ceptometer (Decagon Devices, Inc., Pullman, WA, USA) was placed perpendicular to the transect line under the canopy to measure light intercepted in the plant canopy. This equipment is a lightweight, portable photosythetically active radiation (PAR) sensor that consists of 80 sensors, spaced 1cm apart with a data storage capacity of 1MB RAM (over 2,000 measurements) and provides minimum spatial resolution of 1 cm. It measures canopy gap fraction and calculates LAI by measuring the difference between light levels above the canopy and at ground level. The data obtained from the AccuPAR LP-80 was used to map LAI by combining them with remotely sensed images. This sampling design provided the LAI measurement data at multiple spatial resolutions that were consistent with the pixels sizes of the used aerial photo, TM and MODIS images.

The PAR value were recorded by keeping the probe outside of canopy cover to make sure that it fully received incoming solar radiation that intercepted in tree canopy region. For measuring the PAR valued in shrubs and small trees, the external sensor was mounted above its canopy to determine the solar flux. The AccuPAR plant Ceptometer was placed beneath the canopy layer that measured the radiation beneath the canopy region. Eventually those LAI values were obtained from LP-80 plant ceptometer that measures the difference between light levels above the canopy and at ground level. From each of the sample plots, 5 LAI values were recorded. Mathematically, the in situ LAI relationship derived from the AccuPAR instrument is given by:

$$\mathrm{L} = \frac{\left[\left(1-\frac{1}{2k}\right)fb-1\right]ln\tau}{A(\,1-0.47fb)} \qquad (5)$$

where τ is the ratio of PAR measured below the canopy to PAR above the canopy, f is the beam fraction of incident PAR, K is the extinction coefficient and A is the leaf absorptivity in canopy. This AccuPAR instrument employs this equation in order to calculate LAI automatically. The measurements vary depending on several parameters including local time, date, leaf distribution parameter, zenith angle, and beam fraction.

Assuming the LAI value for each vegetation type, (forest >=5, shrubs/crops = 3-5, grassland 1-3, and baresoil=<1) each grid cell of size 30m were measured. Due to mixed type of vegetation in southern Illinois, the LAI value observed was not observed in consistent fashion. That said, within a closed interval of 6m to next transect line, patches and dispersed type of plant canopy was noticed.

3.5.2 CALCULATION OF LAI MEASUREMENTS

A total of 875 field LAI in situ measurements were obtained over the 5 km × 5 km study region in the heterogeneous landscape. The vegetation canopies of the study area included bare soil that had low LAI value, grasslands and shrubs that had medium LAI values and forests that had high LAI values. There were 5 LAI values to be collected and each matched the pixel value of 1 m resolution aerial photo. The 5 LAI values for each sample plot were averaged to get the mean LAI value that matched the pixel values of 30 m resolution TM image. Similarly, to obtain the LAI value for each 250m, 500m, and 1000m block, the corresponding mean values of 3 sample plots, 5 sample plots, and 7 sample plots were calculated respectively to comply with the pixel values of Landsat TM and MODIS images at 250 m, 500 m, and 1000 m spatial resolution. This aggregation of field data from 30m resulted in a total of 25 LAI average values for each of the spatial resolution. The corresponding central coordinate for each LAI value was obtained and used to extract the pixel values of the remotely sensed images.

3.6 CORRELATION AND REGRESSION MODELING

The ultimate aim of this methodology was to build regression models at multiple spatial resolutions. The extraction of spectral variables was very important. To do so, various image transformations were calculated and would be listed in the section of results. Typical examples for the image transformations were simple ratio (NIR/R), Normalized Difference Vegetation Index (NDVI) (NIR – R / NIR + R), Enhanced Vegetation index (EVI: $G \times (\rho_{NIR} - \rho_{\mathrm{Red}})/(\rho_{NIR} + C_1\rho_{\mathrm{Red}} - C_2\rho_{Blue}) + L$), and Ratio Vegetation Index (RVI: Red / NIR) (Rouse et al. 1974; Jordan 1969; Huete et al. 1996). The purpose of calculating the image transformation was to mitigate the effects of topographic features (slope and aspect) and atmosphere and thus increase the correlation of the images with LAI. Using the central coordinates of the sample plots, the pixel values of all the bands and their transformed images for the aerial photo, Landsat TM and MODIS images were extracted using extraction tool from ArcGIS (Esri, Redlands, CA). Pearson product moment correlation coefficients between the original images and transformed images and the in situ LAI measurements at collected locations were calculated. The correlation coefficients were statistically tested for their significant differences from zero using the equation: $r_\alpha = \sqrt{t_\alpha^2 / (n - 2 + t_\alpha^2)}$ based on the student's distribution at a risk level α = 5%, where *n* is number of sample plots used.

Regression analysis has been widely used for modeling the relationship between spectral variables and LAI (Chen & Cihar 1996; Turner et al. 1999; Cohen et al. 2003). In this study, it was assumed that linear relationship of LAI with the spectral variables was significant at a risk level of 5% at each spatial resolution. Multivariate regression has the following format:

$$Y = \beta_0 + \beta_1 X_1 + \ldots \beta_i X_i + \ldots + \beta_p X_p + \varepsilon \qquad (6)$$

Where Y is the LAI, β_0, is the intercept, β_i are regression coefficients for spectral variable X_i. ε represents the random error - difference between the values estimated by the model and the LAI observations. p is the number of spectral variables.

The regression models were developed to account for the relationships of LAI in situ measurements with spectral variables (original images and their transformations) for the aerial photo, Landsat TM images, and MODIS images at multiple spatial resolutions. For the aerial photo and Landsat TM images, a total of 175 LAI sample plots were available and the sample plots were divided into two sets with 125 plots and 50 plots respectively. The 125 plots were used to develop regression models and the rest 50 plots to assess the accuracy of the resulting LAI maps. For the MODIS images, a total of 25 LAI average values were available and all of them were used for building regression models while the accuracy of the resulting maps was assessed using a cross-validation method to be described in the section of accuracy assessment.

Moreover, all the regression models were generated using multivariate step-wise algorithm that helps select the spectral variables that had significant correlation with LAI at a risk level of 5%. When the stepwise regressions were conducted, the spectral variables were selected based on the significance of regression variances. The significant test of variance was made based on the following criteria. When the probability of F distribution was equal to or less than 0.05, a spectral variable was selected. When the probability was equal to or larger than 0.1, the spectral variable was removed. In addition, the spectral variables that had a correlation coefficient larger than 0.9 with at least one of other spectral variables that were involved in the regression model was removed. The reason of removing the larger coefficient of the variable involved in the model provides an opportunity of less duplication and homogeneity between similar spectral variables. Therefore values of spectral variable with less correlation coefficient were substituted for the other one to get the best regression model. Regression models were built for every resolution image in order to find an accurate site-specific relationship between the measured LAI and spectral variables. The statistical coefficients of multiple determinations (R^2) were output. The models obtained were used to generate LAI maps. The regression modeling was conducted using a statistical software R studio (Rstudio, Boston, MA).

3.7 ACCURACY ASSESSMENT OF MODELS

In this study, the obtained regression models were assessed in several ways. First of all, the statistical coefficients of multiple determinations (R^2) were used. Secondly, a RMSE between the observed and estimated LAI values was calculated for each model and furthermore relative RMSE was obtained by dividing the RMSE with the LAI sample mean. For the aerial photo and Landsat TM images, a total of 50 sample plots were randomly selected from the 175 sample plots and used to assess the accuracy of the resulting models. For the MODIS images, a cross-validation method was used at each spatial resolution. In the cross-validation process, out of 25 random sample plots, initially 5 sample plots were randomly generated for first group cross validation and the model was obtained using the rest 20 sample plots. The obtained model was applied to validate the LAI estimates of the selected 5 sample plots. Similarly, out of remaining 20 sample plots, next 5 sample plots were generated for second group to perform second cross validation. Previously selected sample plots were placed back in the sample pool to develop the second model for cross validation. This process was repeated 5 times and a total of 25 LAI estimates were obtained and used to assess the quality of the model.

CHAPTER 4

RESULTS

4.1 HIGH RESOLUTION: AERIAL PHOTO

A total of 175 collected sample plots were extracted to get the pixel values of the aerial photo derived spectral variables and the correlation coefficients of LAI with the spectral variables are listed in Table 1. In addition to three bands, a total of 21 ratios of bands or band groups were calculated. Based on the t student distribution, the significant correlation coefficient was 0.159 at the risk level of 5%. Obviously, all the correlation coefficients were significant except for the ratio Red/Green+Blue/Green. The highest correlations were 0.51 and 0.50 and obtained using (Red-blue)*Green and (Red-Green)*Blue, respectively.

Table 1: Correlation coefficients between LAI and aerial photo derived spectral variables.

Band	**Correlation**	**Band**	**Correlation**
Blue	-0.43	Blue+Green	-0.42
Green	-0.41	Blue+Green+Red	-0.41
Red	-0.36	blue+Red	-0.41
Blue/Red	-0.44	Green+Red	-0.39
Blue/Green	-0.37	(Blue+Green)/Red	-0.40
Green/Red	-0.32	(Green/Red)*Blue	-0.45
Red/Green	0.31	(Red/Green)-Blue	0.43
Red-Green	0.43	(Red-Blue)/Green	0.42
Red-Blue	0.49	(Red-Green)/Blue	0.27
(Red-blue)*Green	0.51	(Blue/Red)+Green	-0.41
(Red-Green)*Blue	0.50	Green/Red+Blue/Red	-0.40
Red*Green	-0.42	Red/Green+Blue/Green	0.03

All the spectral variables from the 1m resolution aerial photo were input the multivariate regression and the stepwise regression led to a model:

$$LAI = 4.99 + 0.12band2 - 0.11(band3 - band2) * band1 + 0.0012(band1 + band2 + band3) \qquad (7)$$

This model had a low coefficient of determination ($R^2 = 0.23$) and a relative RMSE error of 39.7% with a residual error of 1.81. Figure 7 shows the validation results using 50 sample plots and most of the LAI values were underestimated and few were overestimated, which led to a larger residual error. The linear model didn't show a good fit between the observed and estimated LAI values because only 23 percent of the variation in the LAI was explained by the model.

This model was used to create a LAI map at 1 m resolution (Figure 8) that shows that the LAI estimates had a relative small spatial variability over the heterogeneous area. The LAI estimates for most of the pixels ranged from 4.4 to 5.63 and considerable LAI estimates also had a range of 3.6 - 4.2 (Figure 8). The higher LAI estimates indicated the forested areas. There were some areas in which the LAI estimates were smaller than 3.5, implying the presence of shrubs and lower canopy biomass.

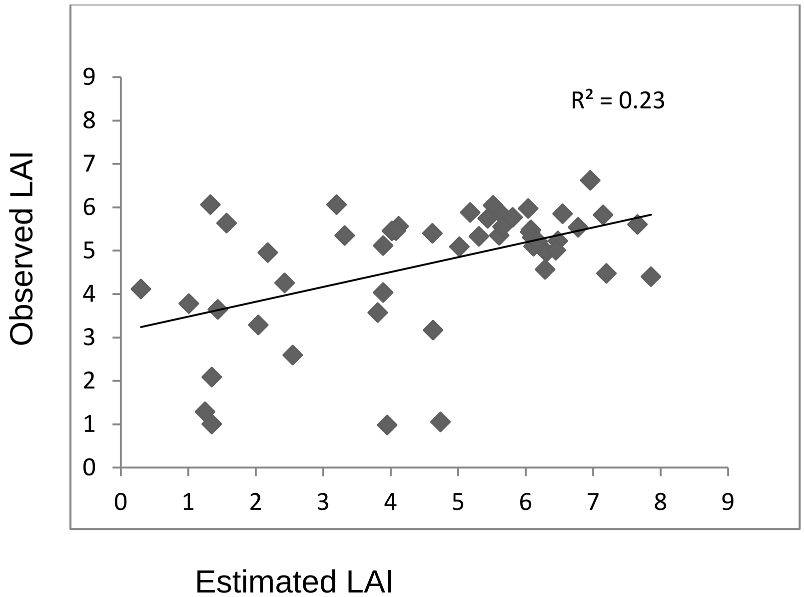

Figure 7: Relationship between observed and estimate LAI values at the 1 m resolution aerial photo.

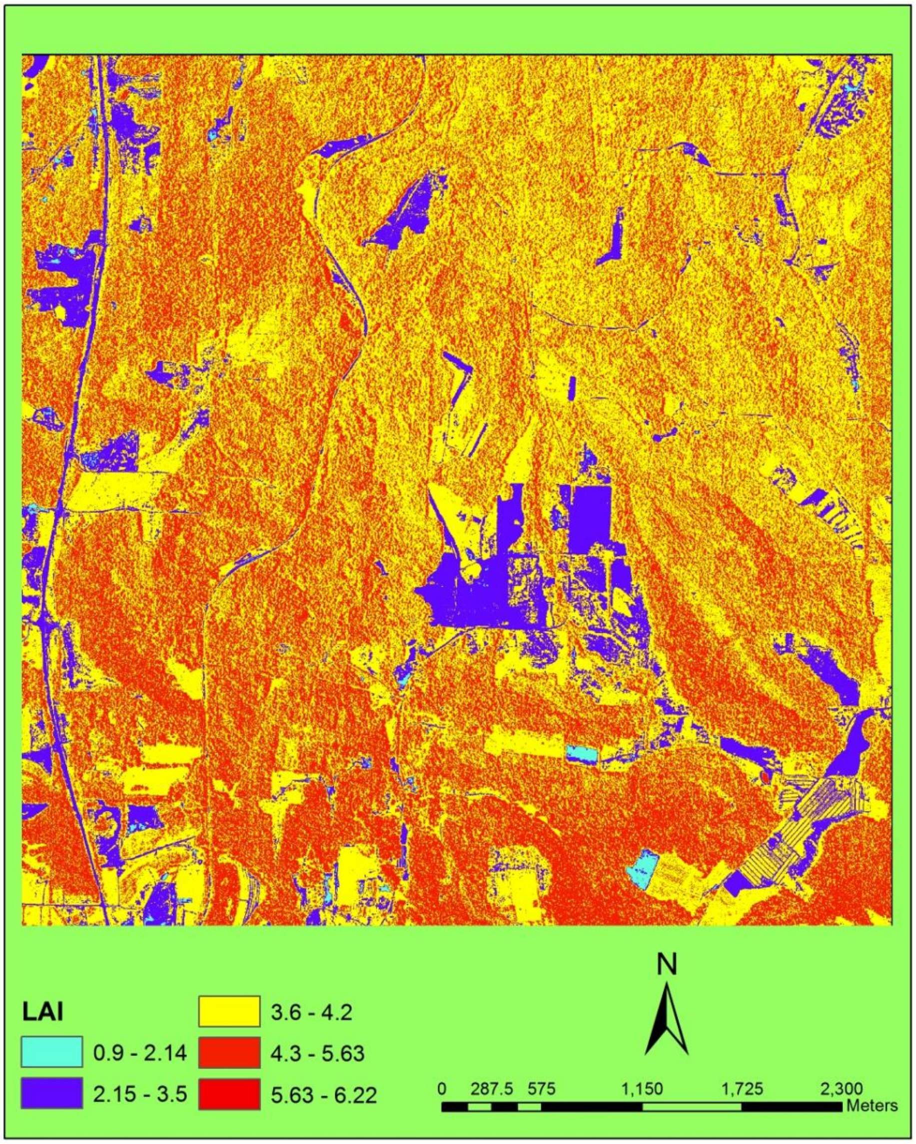

Figure 8: Aerial photo derived LAI map at 1m resolution.

4.2 MEDIUM RESOLUTION: TM IMAGES

A total of 30 ratios of bands and band groups were calculated using the TM bands. The absolute correlation coefficients of the TM derived spectral variables with LAI ranged from 0.18 to 0.71. Based on the significant values 0.159 at a risk level of 5%, all the coefficients were statistically significantly different from zero. The original TM band 5, band 1 and band 7 and their transformations appeared highly correlated with the LAI observations (Table 2). Obviously, three widely used vegetation indices including the simple ratio (SR: NIR/Red), NDVI, and EVI did not show the highest correlation with LAI and they were removed from the obtained model. The multivariate stepwise regression resulted in a model at the 30 m resolution:

$$LAI = 45.52 - 1.29TM5 + 1.56TM7 - 47.41(TM7/TM5) - 60.39/TM7 \qquad (8)$$

This model had a relative RMSE of 25.4% and a coefficient $R^2 = 0.61$ of determination with a residual error of 1.1. The 50 sample plots were used to validate the regression model generated from 125 sample plots. That is, 61 percent of the variation in the LAI was explained by the spectral variables (Figure 9). Compared to the results from the aerial photo at the 1 m resolution, the predictions from this model were more reasonable although few over- and under-estimates took place. The LAI map developed from this model showed considerable variation of LAI values over the landscape (Figure 10). The predicted values ranged from 0.18 to 7.29. The lowest value was observed along the roads and within the bare lands. The higher LAI values dominated the forested areas.

Table 2: Correlation coefficients of LAI with TM image derived spectral variables at the spatial resolution of 30 m.

Bands	**Correlation**	**Bands**	**Correlation**	**Bands**	**Correlation**
TM1	-0.67	TM7/TM5	-0.60	(TM5-TM1)*TM1/TM5	-0.69
TM2	-0.64	TM1/TM7	0.18	TM5+TM7	-0.70
TM3	-0.64	TM4/TM7	0.58	(TM5+TM7)-TM1	-0.70
TM4	0.39	TM5/TM7	0.58	(TM5-TM7/TM1)	-0.71
TM5	-0.71	1/TM1	0.63	(TM5-TM1)/TM5*TM1	0.62
TM7	-0.66	1/TM2	0.57	TM5-(TM1/TM7)	-0.71

SR	0.43	1/TM5	0.68	TM7-(TM5/TM1)	-0.67
NDVI	0.63	1/TM7	0.66	(TM5/TM2-TM7/TM5	-0.71
EVI	0.55	TM(2+4+5)/7	0.58	TM5*TM1/TM7	-0.66
TM1/TM4	-0.62	TM(2+3+5)/4	-0.62	TM5*TM1/TM5	-0.67
TM2/TM4	-0.63	TM(2+3+7)/4	-0.62	(TM5/TM4)+TM7	-0.66
TM3/TM4	-0.61	TM5*TM4	-0.65	TM7/TM5-TM2	0.64
TM5/TM4	-0.59	TM(4-5)/(4+5)	0.59	TM7/TM2-TM5	0.71
TM7/TM4	-0.60	TM(4-7)/(4+7)	0.62	TM5/TM4-TM5/TM7	-0.61
TM1/TM5	-0.55	TM(4/5)/(4/7)	-0.60	TM7/TM3-TM5	0.71
TM2/TM5	-0.42	TM(4/5)+(4/7)	0.58	TM7/TM1-TM5	0.71
TM3/TM5	-0.55	TM(4/7+2/4)	0.57	TM7/TM4-TM5	-0.71
TM4/TM5	0.57	TM5-TM1	-0.72	TM7/TM5-TM1	0.67

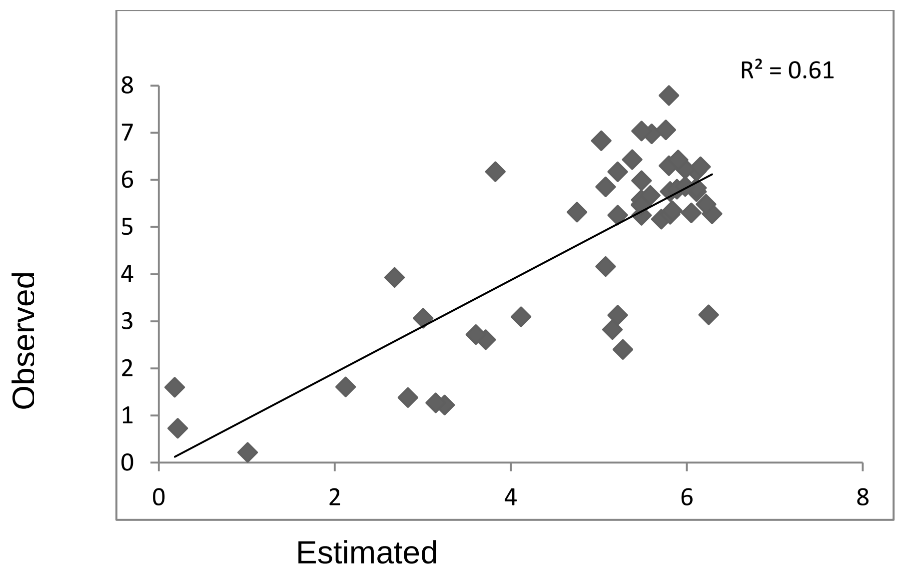

Figure 9: Relationship between observed and estimate LAI values at the 30m resolution of TM image.

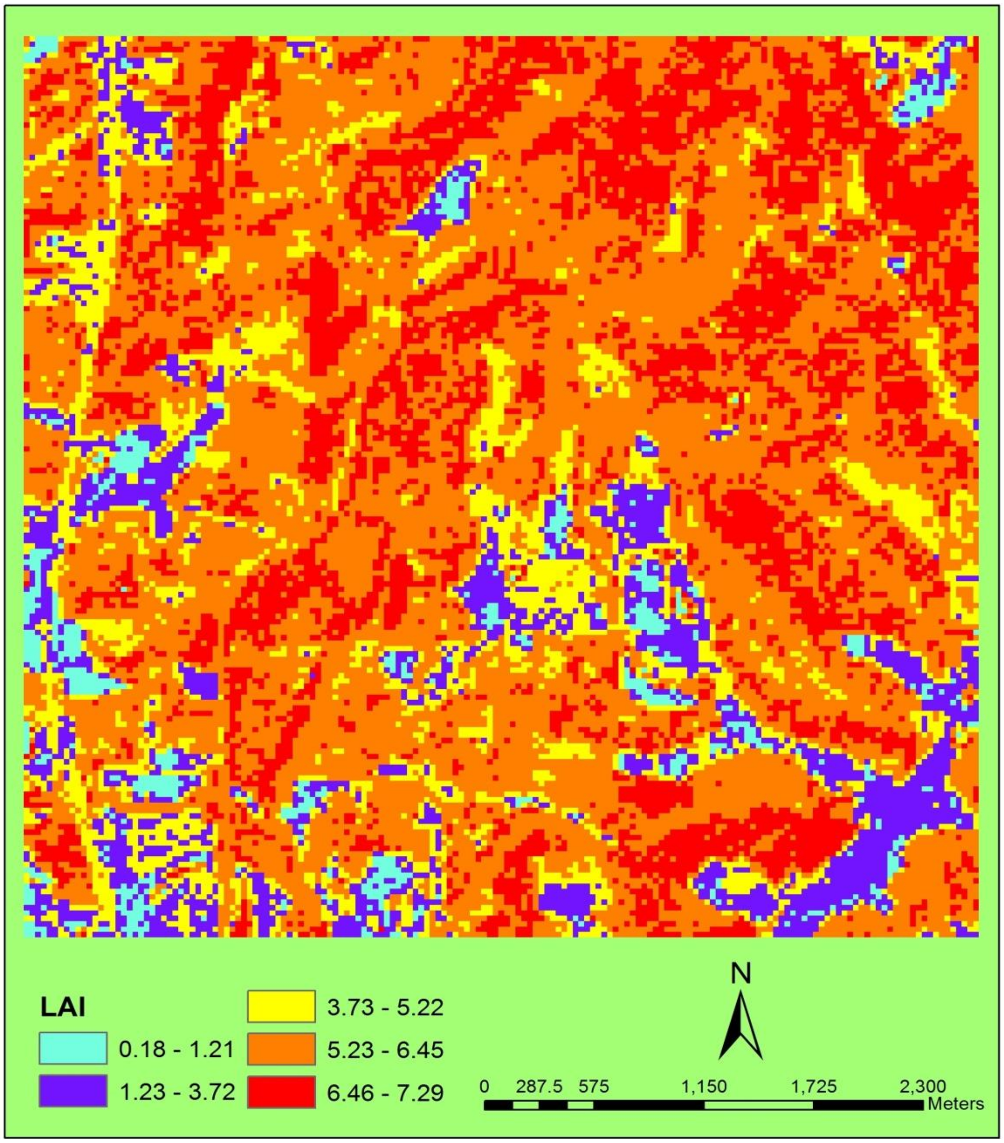

Figure 10: TM image derived LAI map at 30m resolution.

4.2.1 AGGREGATED TM IMAGES

The TM images at the 30 m resolution were aggregated to spatial resolutions of 90 m, 250 m, 500 m, and 1 km. At the 90 m resolution, the absolute correlation coefficients of the spectral variables with LAI varied from 0.33 to 0.64. Although all the coefficients were statistically significant (larger than 0.159 at a risk level of 5%), the coefficients were slightly smaller than those at the original 30 m resolution (Table 3). The correlation coefficients continuously became slightly smaller when the aggregated TM images had spatial resolutions of 250 m and 500 m (Table 4 and Table 5). When the spatial resolution was 1 km, the absolute correlation coefficients ranged from 0.01 to 0.47 and became much smaller (Table 6). This implied the aggregation of TM images decreased their correlations with LAI. Moreover, three widely used vegetation indices did not show the highest correlation with LAI at all the spatial resolutions.

Table 3: Correlation coefficients of LAI with the aggregated TM images at the spatial resolution of 90 m.

Bands	**Correlation**	**Bands**	**Correlation**	**Bands**	**Correlation**
TM1	-0.60	TM7/TM5	-0.65	(TM5-TM1)*TM1/TM5	-0.64
TM2	-0.60	TM1/TM7	0.38	TM5+TM7	-0.63
TM3	-0.57	TM4/TM7	0.50	(TM5+TM7)-TM1	-0.63
TM4	0.55	TM5/TM7	0.63	(TM5-TM7/TM1)	-0.61
TM5	-0.62	1/TM1	0.51	(TM5-TM1)/TM5*TM1	0.50
TM7	-0.63	1/TM2	0.47	TM5-(TM1/TM7)	-0.62
SR	0.33	1/TM5	0.57	TM7-(TM5/TM1)	-0.63
NDVI	0.57	1/TM7	0.58	(TM5/TM2-TM7/TM5	-0.62
EVI	0.52	TM(2+4+5)/7	0.53	TM5*TM1/TM7	-0.50
TM1/TM4	-0.57	TM(2+3+5)/4	-0.57	TM5*TM1/TM5	-0.60
TM2/TM4	-0.60	TM(2+3+7)/4	-0.60	(TM5/TM4)+TM7	-0.63
TM3/TM4	-0.57	TM5*TM4	-0.57	TM7/TM5-TM2	0.59
TM5/TM4	-0.52	TM(4-5)/(4+5)	0.50	TM7/TM2-TM5	0.62
TM7/TM4	-0.60	TM(4-7)/(4+7)	0.61	TM5/TM4-TM5/TM7	-0.62
TM1/TM5	-0.50	TM(4/5)/(4/7)	-0.65	TM7/TM3-TM5	0.61
TM2/TM5	-0.47	TM(4/5)+(4/7)	0.49	TM7/TM1-TM5	0.61
TM3/TM5	-0.48	TM(4/7+2/4)	0.49	TM7/TM4-TM5	-0.62
TM4/TM5	0.43	TM5-TM1	-0.62	TM7/TM5-TM1	0.59

Table 4: Correlation coefficients of LAI with the aggregated TM images at the spatial resolution of 250 m.

Bands	Correlation	Bands	Correlation	Bands	Correlation
TM1	-0.65	TM4/TM5	0.52	TM(4-5)/(4+5)	0.56
TM2	-0.64	TM7/TM5	-0.66	TM(4-7)/(4+7)	0.64
TM3	-0.65	TM1/TM7	0.09	TM(4/5)/(4/7)	-0.66
TM4	-0.30	TM2/TM7	0.01	TM(4/5)+(4/7)	0.56
TM5	-0.66	TM3/TM7	-0.33	TM(4/5+2/4)	0.47
TM7	-0.67	TM4/TM7	0.57	TM(4/7+2/4)	0.56
SR	0.35	TM5/TM7	0.64	TM5-TM1	-0.65
NDVI	0.61	1/TM1	0.46	TM5-TM7	-0.33
EVI	0.56	1/TM2	0.44	TM5+TM7	-0.67
TM1/TM4	-0.62	1/TM3	0.31	TM7+TM5/TM4	-0.61
TM2/TM4	-0.64	1/TM4	0.24	(TM5-TM7)/TM5	0.66
TM3/TM4	-0.63	1/TM5	0.54	TM5+TM7/TM7	0.64
TM5/TM4	-0.57	1/TM7	0.56	(TM5/TM4)+TM7	-0.67
TM7/TM4	-0.64	TM(2+3+5)/7	0.55	(TM5-TM4)/(TM+TM4)	-0.56
TM1/TM5	-0.58	TM(2+4+5)/7	0.59	(TM5-TM4)/(TM4)	-0.57
TM2/TM5	-0.52	TM(2+3+5)/4	-0.61	TM5+TM7/TM5	-0.66
TM3/TM5	-0.56	TM(2+3+7)/4	-0.64		
		TM5*TM4	-0.58		

Table 5: Correlation coefficients of LAI with the aggregated TM images at the spatial resolution of 500 m.

Bands	Correlation	Bands	Correlation	Bands	Correlation
TM1	-0.58	TM4/TM5	0.39	TM(4-5)/(4+5)	0.41
TM2	-0.60	TM7/TM5	-0.59	TM(4-7)/(4+7)	0.52
TM3	-0.58	TM1/TM7	0.08	TM(4/5)/(4/7)	-0.59
TM4	-0.37	TM2/TM7	-0.08	TM(4/5)+(4/7)	0.46

TM5	-0.57	TM3/TM7	-0.30	TM(4/5+2/4)	0.34
TM7	-0.59	TM4/TM7	0.48	TM(4/7+2/4)	0.47
SR	0.30	TM5/TM7	0.58	TM5-TM1	-0.56
NDVI	0.51	1/TM1	0.39	TM5-TM7	-0.26
EVI	0.50	1/TM2	0.39	TM5+TM7	-0.58
TM1/TM4	-0.49	1/TM3	0.25	TM7+TM5/TM4	-0.47
TM2/TM4	-0.54	1/TM4	0.28	(TM5-TM7)/TM5	0.59
TM3/TM4	-0.51	1/TM5	0.45	TM5+TM7/TM7	0.58
TM5/TM4	-0.42	1/TM7	0.48	(TM5/TM4)+TM7	-0.58
TM7/TM4	-0.51	TM(2+3+5)/7	0.47	(TM5-TM4)/(TM+TM4)	-0.41
TM1/TM5	-0.52	TM(2+4+5)/7	0.50	(TM5-TM4)/(TM4)	-0.42
TM2/TM5	-0.54	TM(2+3+5)/4	-0.48	TM5+TM7/5	-0.59
TM3/TM5	-0.52	TM(2+3+7)/4	-0.52		
		TM5*TM4	-0.57		

Table 6: Correlation coefficients of LAI with the aggregated TM images at the spatial resolution of 1km.

Bands	**Correlation**	**Bands**	**Correlation**	**Bands**	**Correlation**
TM1	-0.17	TM4/TM5	0.35	TM(4-5)/(4+5)	0.39
TM2	-0.34	TM7/TM5	-0.26	TM(4-7)/(4+7)	0.37
TM3	-0.16	TM1/TM7	-0.27	TM(4/5)/(4/7)	-0.26
TM4	0.23	TM2/TM7	-0.43	TM(4/5)+(4/7)	0.32
TM5	0.03	TM3/TM7	-0.29	TM(4/5+2/4)	0.28
TM7	-0.04	TM4/TM7	0.31	TM(4/7+2/4)	0.29
SR	0.33	TM5/TM7	0.27	TM5-TM1	0.09
NDVI	0.41	1/TM1	0.18	TM5-TM7	0.10
EVI	0.28	1/TM2	0.39	TM5+TM7	0.01
TM1/TM4	-0.43	1/TM3	0.23	TM7+TM5/TM4	-0.39
TM2/TM4	-0.47	1/TM4	-0.40	(TM5-TM7)/TM5	0.26
TM3/TM4	-0.40	1/TM5	-0.27	TM5+TM7/TM7	0.27
TM5/TM4	-0.39	1/TM7	-0.08	(TM5/TM4)+TM7	-0.06
TM7/TM4	-0.38	TM(2+3+5)/7	-0.06	(TM5-TM4)/(TM+TM4)	-0.39
TM1/TM5	-0.44	TM(2+4+5)/7	0.27	(TM5-TM4)/(TM4)	-0.39

TM2/TM5	-0.52	TM(2+3+5)/4	-0.43	TM5+TM7/5	-0.26
TM3/TM5	-0.37	TM(2+3+7)/4	-0.43		
		TM5*TM4	0.02		

Table 7 listed the models obtained by multivariate stepwise regression using the aggregated TM images at spatial resolutions of 90 m, 250 m, 500 m, and 1 km. Figure 11 showed the validation results of the models for estimating LAI values for 50 sample plots at these spatial resolutions. It seemed that the spatial resolution of 1 km led to the smallest relative RMSE and highest values of R^2, while the spatial resolution of 250 m resulted in the largest relative RMSE and smallest values of R^2 and the LAI values were seriously underestimated.

Table 7: Regression models and their accuracies for the spectral variables derived from the aggregated TM images at spatial resolutions of 250 m, 500 m, and 1 km, respectively.

Resolution	**MODEL**	**R^2**	**Residual**	**Relative RMSE**
90m	LAI=-82.8+2.19TM7-173.2(TM3/TM4)+61.42(TM5/TM4)+99.37(TM3/TM5)-0.015(TM5*TM4+75.09(TM4-TM7/TM4+TM7)	0.66	0.92	19.8
250m	LAI=6.4152-0.15938*TM7	0.44	1.18	25.3
500m	LAI=-492.91629TM5+2.1723TM5*TM4+0.0301(TM4-TM5/TM4+TM5)+452.20(TM4-TM7/TM4+TM7)+562.49TM7/TM5+484.90TM7/TM4+8.62TM4/TM5+TM4/TM7)	0.56	0.91	18.9
1km	LAI=-13.38+10.57TM5-5.47(TM5-TM1)+1.40(TM7/TM5-TM2) -4.11(TM5/TM4-TM5/TM7)+5.98(TM7/TM1-TM5)	0.67	0.71	14.7

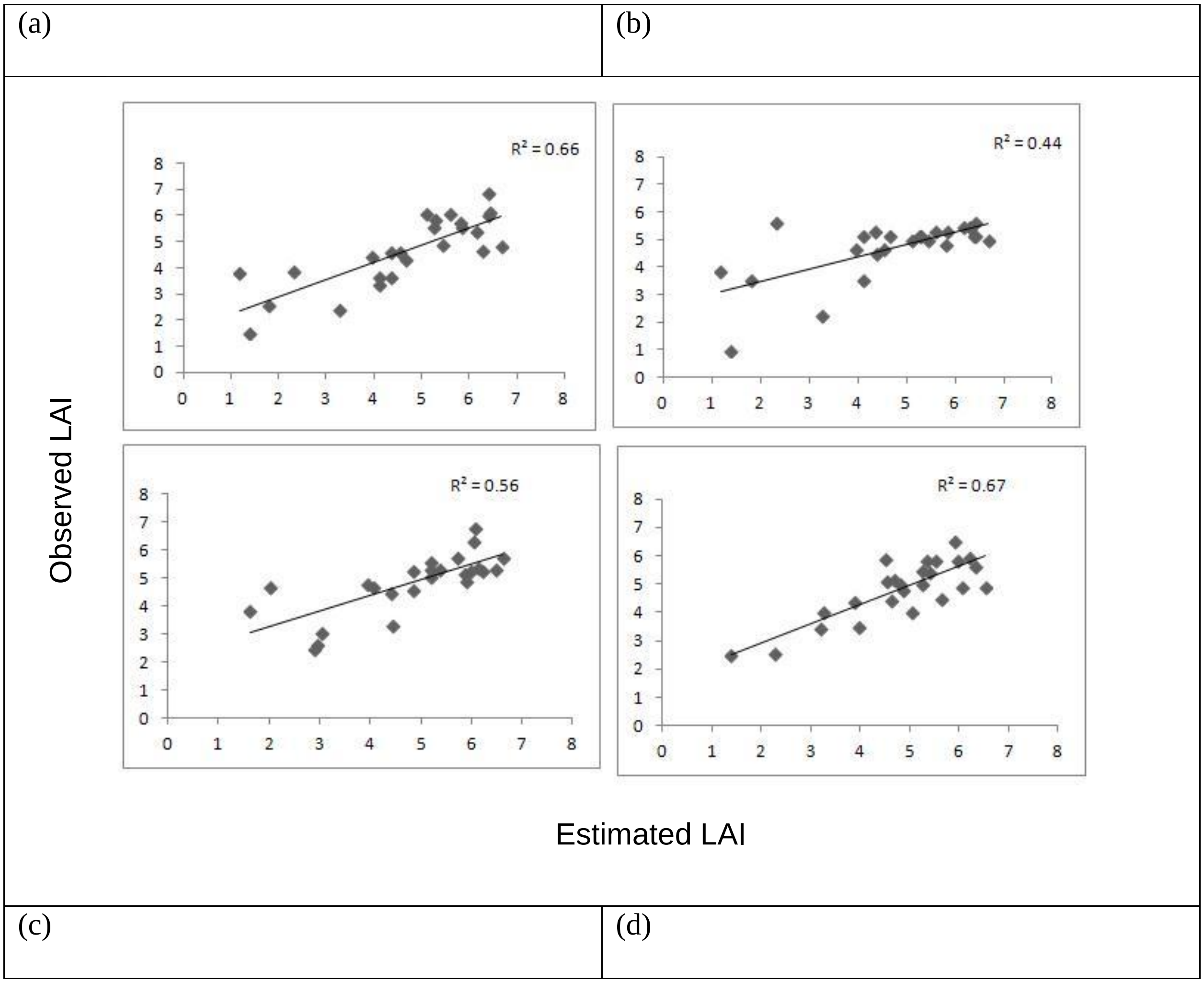

Figure 11: Relationship between observed and estimate LAI values at the spatial resolutions of 90 m, 250 m, 5000 m, and 1 km.

The LAI estimation maps derived using the models from the aggregated TM images at the spatial resolutions of 90 m, 250 m, 500 m, and 1km were presented in Figure 12. The LAI estimates varied from 1 to 6.9. Compared to those at the spatial resolution of 30 m, the minimum estimate got slightly larger and the maximum estimate got slightly smaller, as the spatial resolution became coarser. The LAI estimates were smoothed and their spatial distribution and patterns became not noticeable.

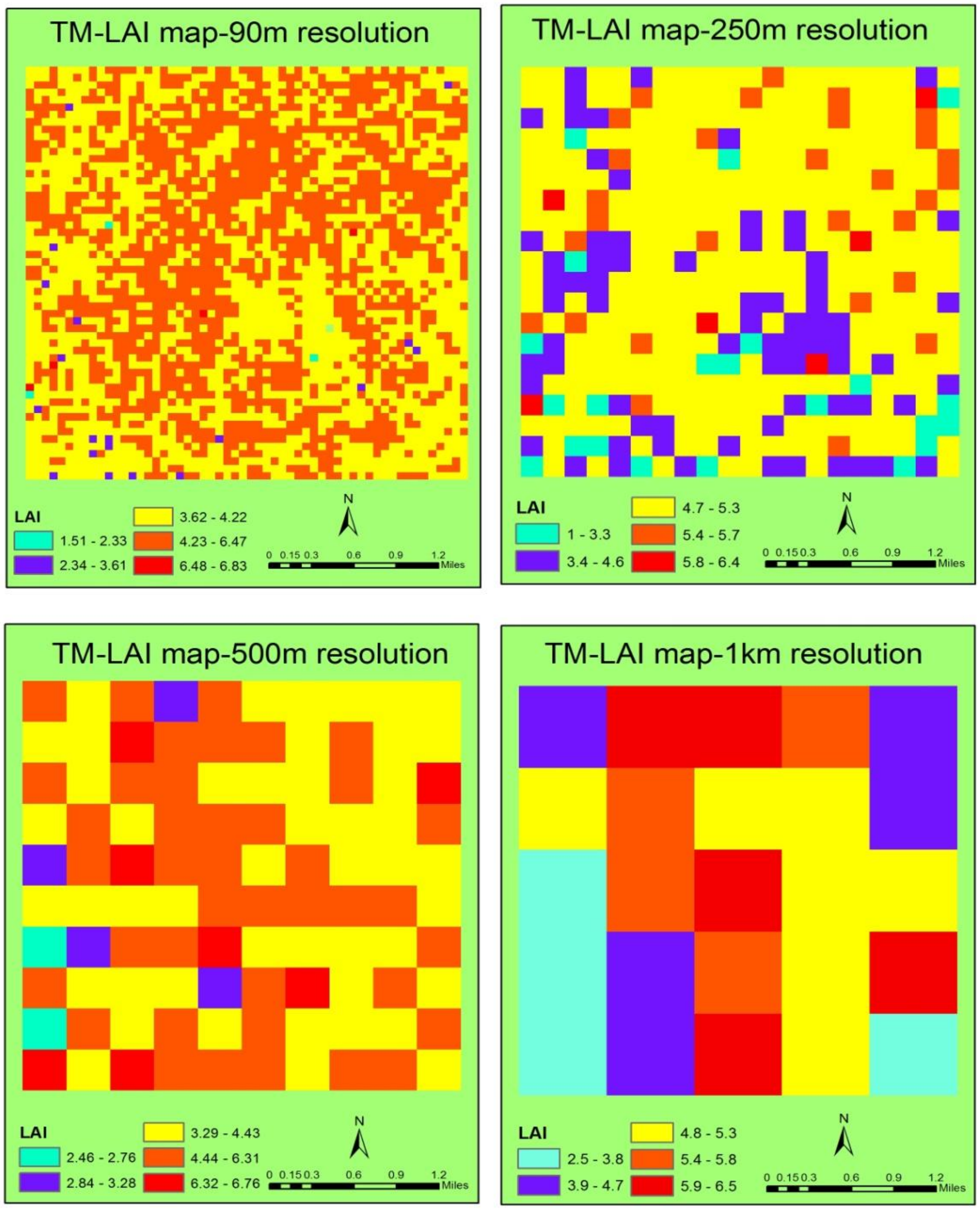

Figure 12: LAI estimation maps using the models obtained using the aggregated TM images at the spatial resolutions of 90 m, 250 m, 500 m, and 1km.

4.3 COARSE RESOLUTION: MODIS IMAGES

The correlation coefficients between the MODIS derived spectral variables and LAI were listed in Table 8, Table 9, and Table 10 for spatial resolutions of 250 m, 500 m, and 1 km, respectively. The highest correlation was -0.51 obtained by blue*red / NIR) at the spatial resolution of 250 m, -0.49 obtained by blue band at the spatial resolution of 500 m, and -0.48 obtained by blue band at the spatial resolution of 1 km. Overall, most of the coefficients were not significantly different from zero at a risk level of 5%. The correlations were much lower than those using TM images and decreased as the spatial resolution became coarser. At the spatial resolution of 250 m, the red channel and its relevant ratios including NDVI and EVI led to higher correlation. At the spatial resolutions of 500 m and 1 km, the blue channel and its relevant ratios resulted in higher correlation and the coefficients from three widely used vegetation indices (SR, NDVI and EVI) became moderate although not significant.

Table 8: Correlation coefficients of MODIS derived spectral variables with LAI at 250 m spatial resolution. The significant value was 0.381 at a risk level of 5% and the symbol * indicate the coefficient is significantly different from zero.

Bands	**Correlation**	**Bands**	**Correlation**
blue	-0.38	1/red	0.00
red	-0.45*	nir/mir	0.14
nir	0.30	mir/nir	-0.24
mir	-0.20	mir*nir	-0.06
ndvi	0.48*	mir-nir/mir+nir	-0.22
evi	0.44*	(mir-red)/mir	-0.14
SR	0.30	(blue+red +nir)/mir	-0.13
		blue+red/nir	-0.42*
blue*red/nir	-0.51*	nir/red+nir/mir	0.26
red/nir	-0.41*	nir/blue	0.41*
1/blue	0.20	nir/red+mir/red	0.29
		mir/blue	0.39*

Table 9: Correlation coefficients of MODIS derived spectral variables with LAI at 500 m spatial resolution. The significant value was 0.381 at a risk level of 5% and the symbol * indicate the coefficient is significantly different from zero.

Bands	Correlation	Bands	Correlation
blue	-0.49*	nir/mir	0.26
red	-0.35	mir/nir	-0.27
nir	0.30	mir*nir	-0.21
mir	-0.26	mir-nir/mir+nir	-0.27
ndvi	0.37	(mir-red)/mir	-0.26
evi	0.36	(blue+red +nir)/mir	-0.01
SR	0.45*	blue+red/nir	-0.42*
		nir/red+nir/mir	0.39*
blue*red/nir	-0.38	nir/blue	0.40*
red/nir	-0.36	nir/red+mir/red	0.47*
1/blue	0.40*	mir/blue	0.25
1/red	0.46*		

Table 10: Correlation coefficients of MODIS derived spectral variables with LAI at 1 km spatial resolution. The significant value was 0.381 at a risk level of 5% and the symbol * indicate the coefficient is significantly different from zero.

Bands	Correlation	Bands	Correlation
blue	-0.48*	1/red	0.33
red	-0.38	nir/mir	0.25
nir	0.35	mir/nir	-0.19
mir	-0.41*	mir*nir	-0.22
ndvi	0.37	mir-nir/mir+nir	-0.38
evi	0.33	(mir-red)/mir	0.01
SR	0.33	(blue+red +nir)/mir	0.21
		blue+red/nir	-0.17
blue*red/nir	-0.14	nir/red+nir/mir	0.30
red/nir	-0.15	nir/blue	0.27
1/blue	0.27	nir/red+mir/red	0.33
		mir/blue	0.25

Three regression models were obtained using the step-wise regression method with all the 25 sample plots (Table 11) and the relationships of the estimated LAI with the observed LAI were shown in Figures 13, 14, and 15, respectively. Although the spatial resolution of 250 m led to the highest coefficient of determination, $R^2 = 0.7$, the spatial resolution of 1 km resulted in the smallest relative RMSE, 17.5%. Three widely used vegetation indices (SR, NDVI and EVI) were involved in the models.

Table 11: Regression models from MODIS derived spectral variables at the spatial resolutions of 250 m, 500 m, and 1 km.

Spatial Resolutions	**Model**	**RMSE**	**Relative RMSE**	**R^2**
MODIS 250m	LAI= -7.81-0.049MIR+0.10EVI-1.36SR+6.33MIR/NIR	0.86	18.54	0.70
MODIS 500m	LAI=26.37-0.32Red+0.48NIR+0.05MIR-0.56EVI-4.45SR-349.64(1/Blue)+1432(1/Red)	0.90	18.79	0.56
MODIS 1km	LAI=2.47+0.02NDVI+5.63(Red/NIR)-0.19(Blue+Red+NIR)/MIR-2.69(Blue+Red)/NIR	0.84	17.52	0.53

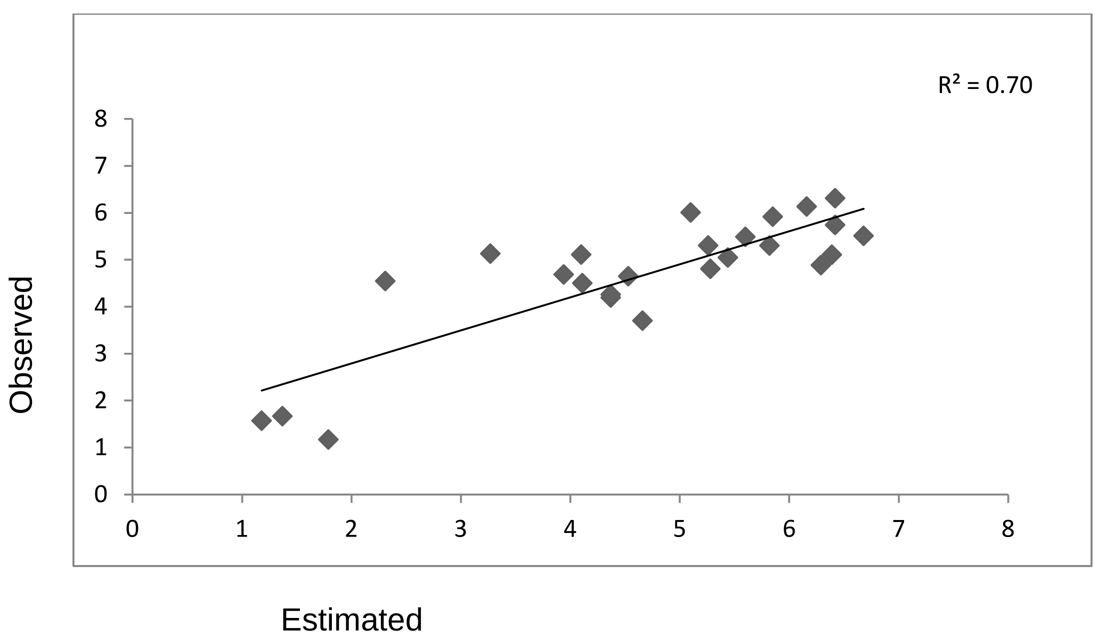

Figure 13: Relationship between the estimated and observed LAI values at the 250 m spatial resolution.

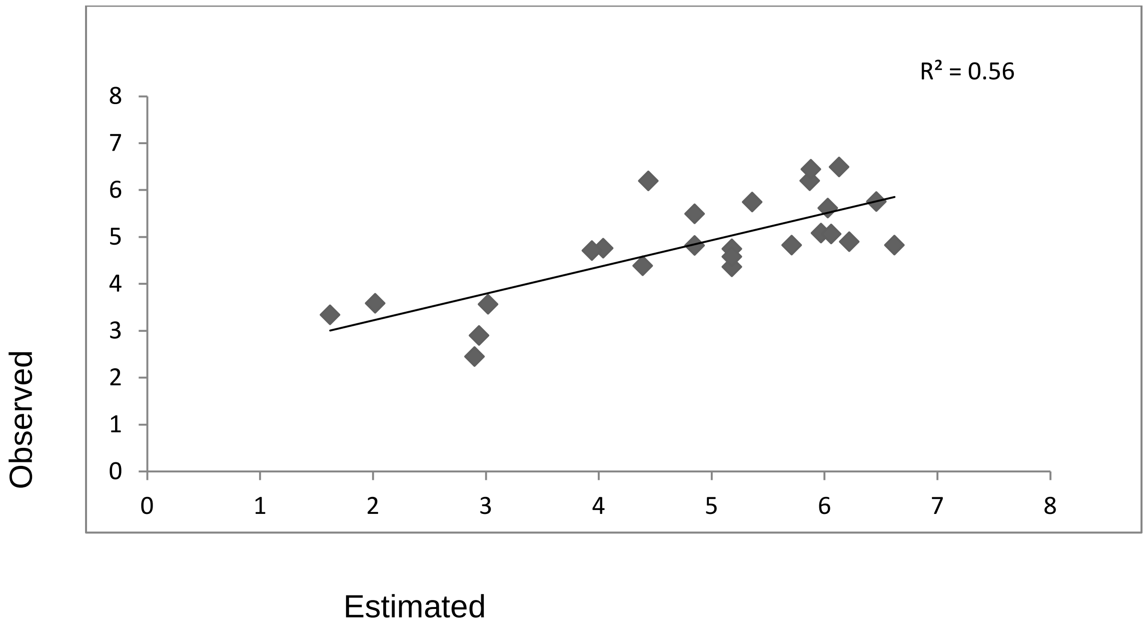

Figure 14: Relationship between the estimated and observed LAI values at the 500 m spatial resolution.

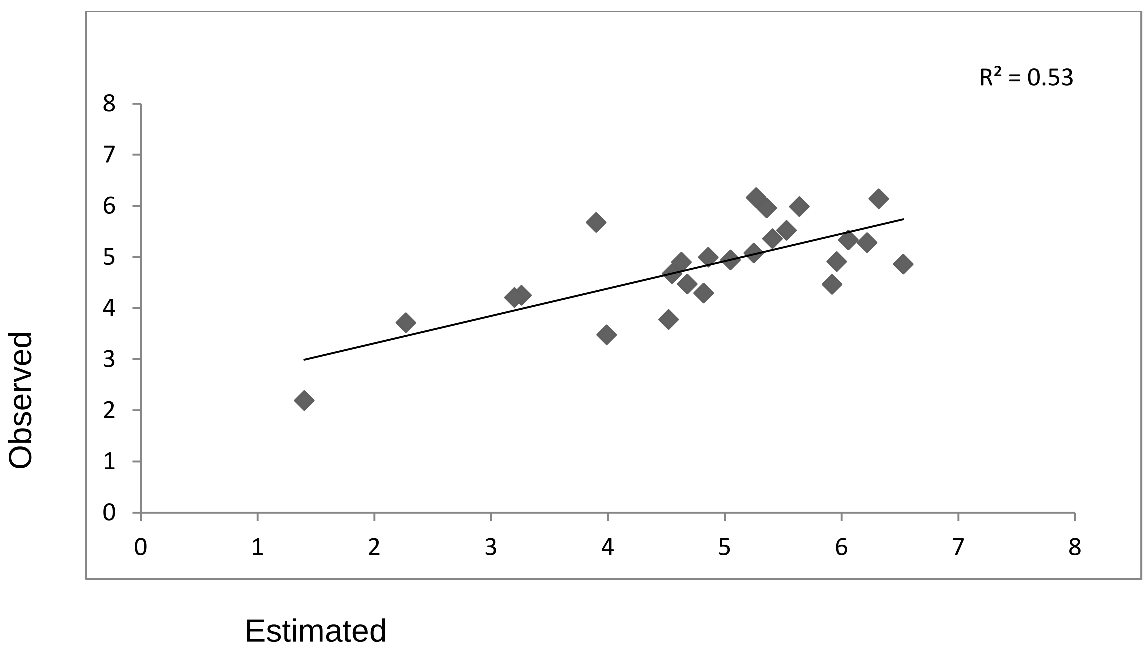

Figure 15: Relationship between the estimated and observed LAI values at the 1 km spatial resolution.

Figure 16 illustrates the LAI estimation maps obtained using MODIS derived spectral variables at three spatial resolutions of 250 m, 500 m, and 1 km. It could be clearly seen that in the LAI map of 250 m spatial resolution, the high LAI values dominated the study area, implying the hardwood forests covered most of the study area. The spatial patterns (Figure 16) were similar to those obtained using the TM images at spatial resolutions of 30 m and 90 m (Figures 10 and 12a). As the spatial resolution became coarser, the spatial patterns of high value clustering eventually disappeared. For comparison, the 1 km resolution MODIS LAI product that was directly downloaded from the website was also shown in Figure 16. The spatial patterns looked slightly different from those obtained using MODIS images at various spatial resolutions in this study.

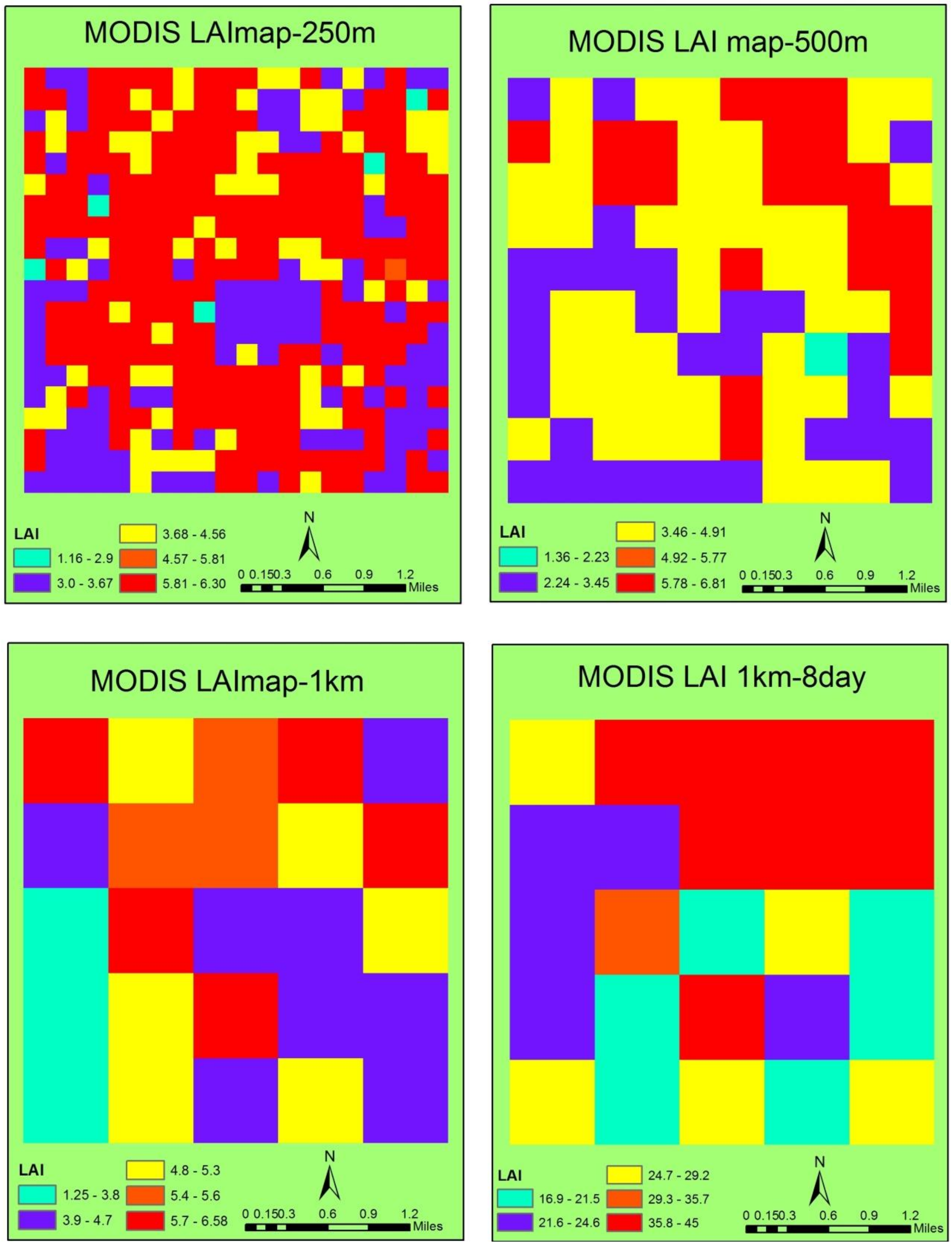

Figure 16: LAI estimation maps obtained using MODIS derived spectral variables at three spatial resolutions of 250 m, 500 m, and 1 km.

The cross validation of MODIS derived models at the spatial resolutions of 250m, 500 m, and 1 km were conducted (Tables 12 to 14 and Figures 17-19). The LAI estimates of all 25 sample plots were validated using the models obtained from five groups each having 20 sample plots. The coefficients of determination varied from 0.56 to 0.93, that is, at least 56 percent of variation could be explained by the spectral variables. The residual ranged from 0.57 to 1.17. Commonly, underestimation occurred and series overestimation and underestimation took place for group 5 at the spatial resolution of 250 m and for group 3 at the spatial resolution of 1 km.

Table 12: Regression models for cross-validation using five groups at the spatial resolution of 250 m.

MODIS-250m	Model	Residual	R2
Group 1	LAI=R+(B*R)/NIR+NIR/MIR	0.57	0.56
Group 2	LAI=B+R+NDVI+EVI+(B*R)/NIR+1/B+1/R+(MIR-R)/MIR+(NIR/R+NIR/MIR)+ MIR/B	0.58	0.59
Group 3	LAI=SR+(B*R)/NIR+1/B+1/R+MIR*NIR+(MIR-NIR)/MIR+(NIR/R-MIR/R)	0.58	0.64
Group 4	LAI=R+(B*R)/NIR+NIR/MIR+MIR/NIR+(MIR-NIR)/MIR	0.82	0.86
Group 5	LAI=NDVI+(MIR-NIR)/MIR+MIR*NIR+(MIR-NIR)/MIR+(NIR/R+MIR/R)	0.91	0.64

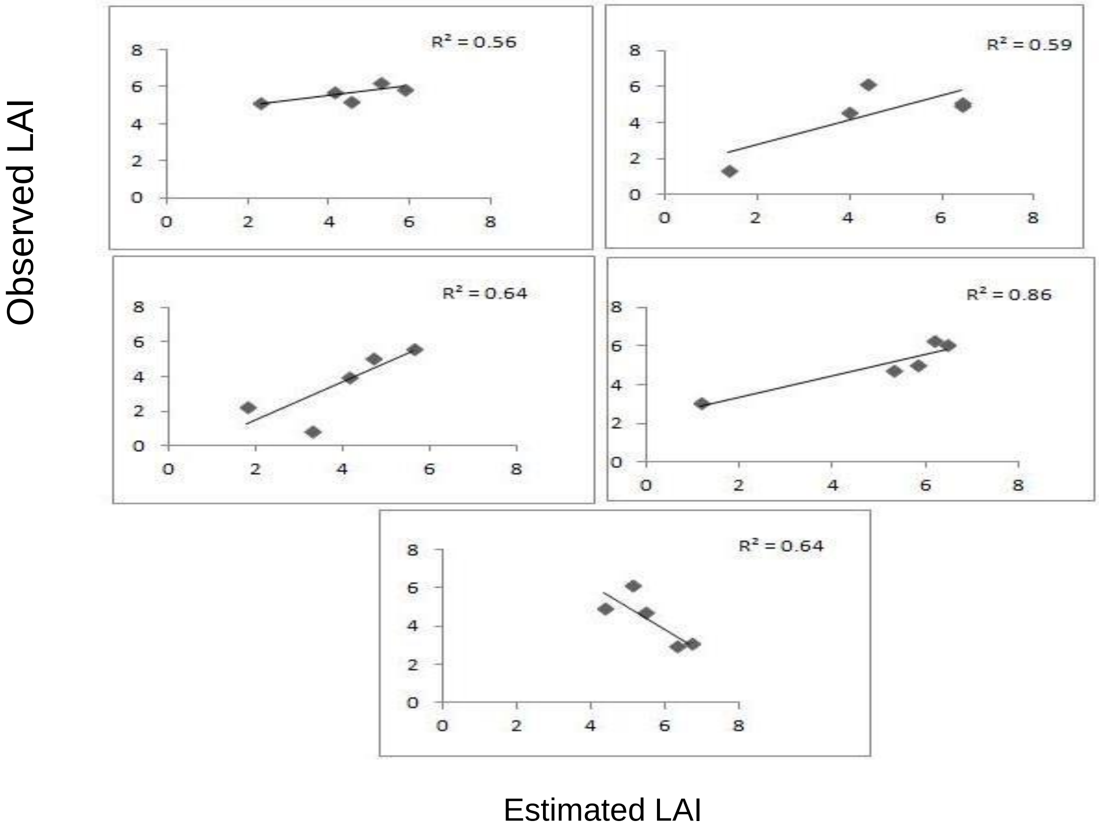

Figure 17: Relationship between observed and estimated LAI values for cross-validation using five groups at the spatial resolution of 250 m.

Table 13: Regression models for cross-validation using five groups at the spatial resolution of 500 m.

MODIS-500m	Model	Residual	R2
Group 1	LAI=SR+1/B+MIR/NIR+(MIR-NIR/MIR+NIR)+(NIR/R+NIR/MIR+NIR/R+MIR/R	1.17	0.62
Group 2	LAI=B+R+NIR+NDVI+EVI+(B*R)/NIR+R/NIR+NIR/MIR+NIR/B	0.71	0.92
Group 3	LAI=R+SR+ MIR/NIR+(B+R)/NIR+NIR/B+MIR/B	1.09	0.87
Group 4	LAI=R+NIR+NDVI+EVI+SR+(B*R)/NIR+1/R+NIR/MIR+(B+R)/NIR	0.76	0.60
Group 5	LAI=SR+MIR*NIR+(MIR-R)/MIR+(B+R)/NIR+(NIR/R+NIR/MIR)+ (NIR/R+NIR/MIR)+ (NIR/B+NIR/R+MIR/R)+ MIR/B	1.0	0.56

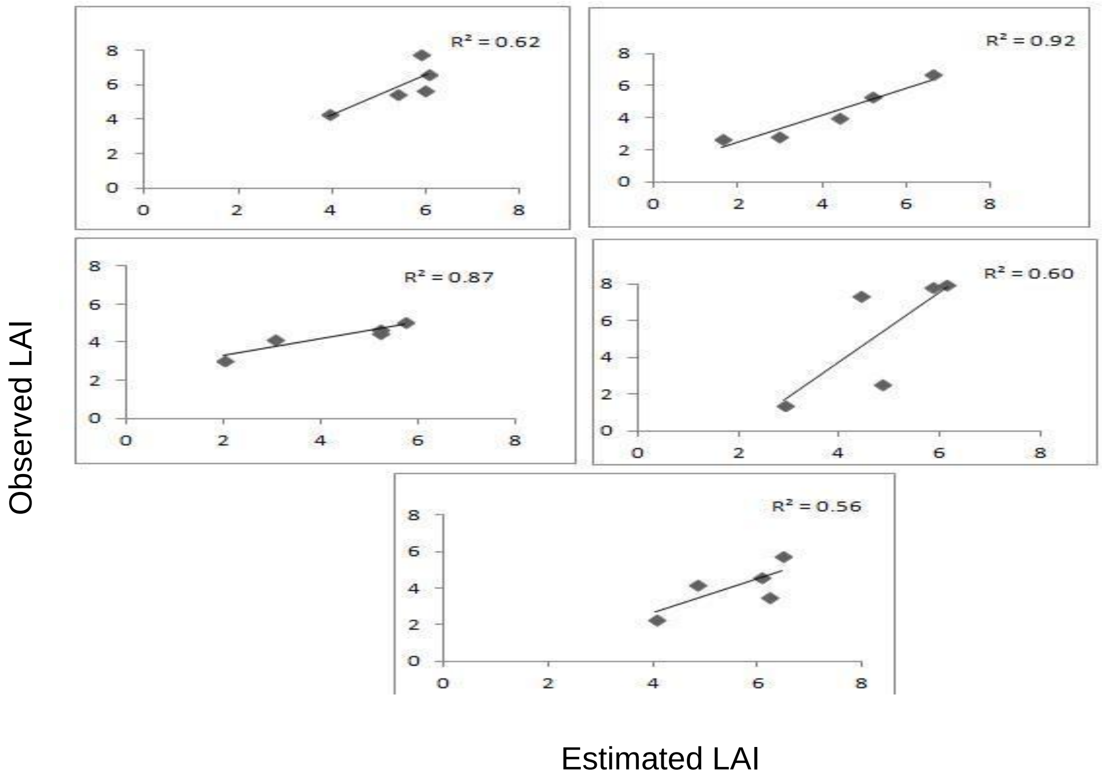

Figure 18: Relationship between observed and estimated LAI values for cross-validation using five groups at the spatial resolution of 500 m.

Table 14: Regression models for cross-validation using five groups at the spatial resolution of 1 km.

MODIS 1000m	Model	Residual	R2
Group 1	LAI=Red+NDVI+SR+EVI+B*R/NIR+1/R+NIR/MIR+(MIR-R)/MIR+(B+R+NIR)/MIR+(B+R)/NIR+(NIR/R+NIR/MIR)+NIR/B+MIR/B	0.49	0.93
Group 2	LAI=B+R+NDVI+EVI+(B*R/NIR)+R/NIR+1/B+1/R+(MIR*NIR)	0.68	0.89
Group 3	LAI=MIR+R/NIR+(MIR-NIR/MIR+NIR)+(B+R+NIR)/MIR+(B+R)/NIR	0.96	0.49
Group 4	LAI=NDVI+R/NIR+(B+R)/NIR+NIR/R+NIR/MIR	1.12	0.60

Group 5	LAI=NDVI+1/blue+(B+R)/NIR+(NIR/R+NIR/MIR)+(NIR/R+MIR/R)	1.07	0.75

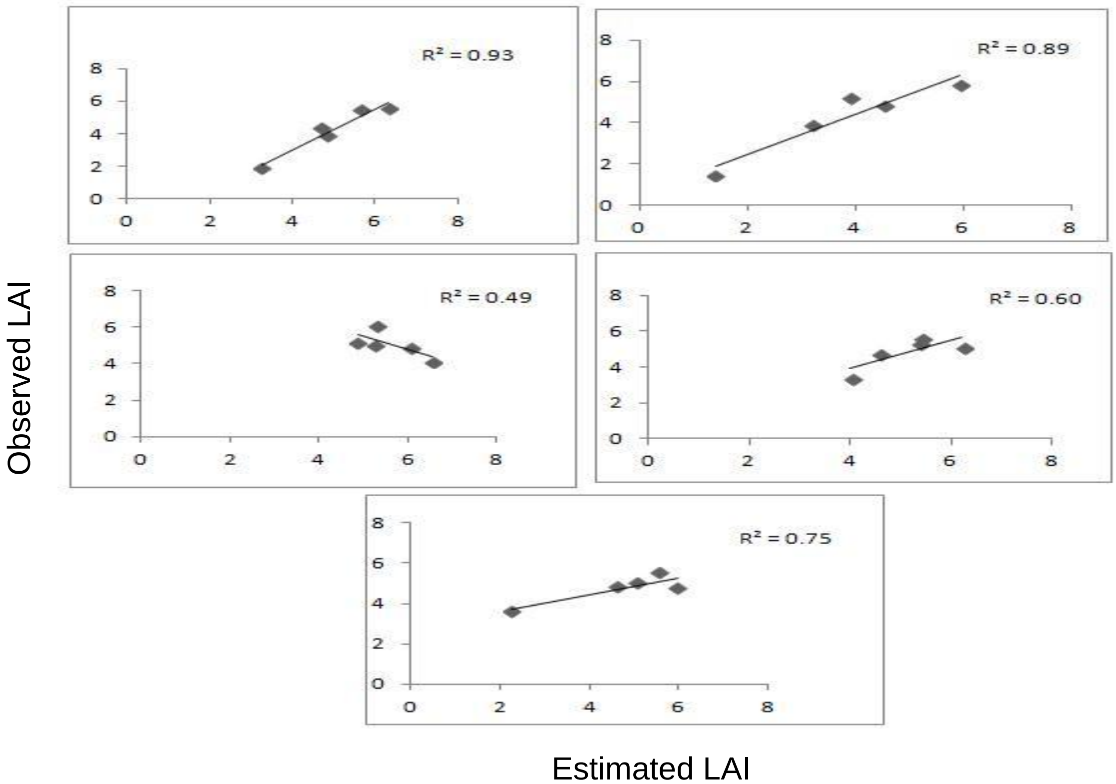

Figure 19: Relationship between observed and estimated LAI values for cross-validation using five groups at the spatial resolution of 1 km.

4.4 COMPARISON OF AERIAL PHOTO, TM AND MODIS DERIVED LAI MAPS

The aerial photo and TM derived LAI products at the spatial resolutions of 1 m and 30 m were scaled up to the spatial resolution of 1 km and compared to that from MODIS derived LAI map in this study. In addition, the MODIS LAI product that was directly downloaded from website was compared in terms of correlation although its values varied from 0 to 255 with high values implying the large LAI and low values the smaller LAI. All the aerial photo, TM and

MODIS derived LAI mean estimates were similar. However, the standard deviation of the aerial photo derived LAI values was much smaller with relatively larger minimum and relatively small maximum (Table 15). The minimum, maximum, and standard deviations from the TM and MODIS derived LAI values were similar. That is, the aerial photo derived LAI maps had series overestimation and underestimation for the smaller LAI values and larger LAI values, respectively.

From the correlation matrix, it was found that there were moderate correlations among the aerial photo, TM and MODIS derived LAI products (Table 15). The correlation coefficients of the aerial photo derived LAI map with MODIS derive LAI map significantly differed from zero based on the significant value 0.381 at a risk level of 5%, its correlation with TM derived LAI map was close to the significant value. The MODIS derived LAI map had a significant correlation with both the TM derived LAI map and the directly downloaded MODIS LAI image. However, both the aerial photo and TM derived LAI products were not significantly correlated with the directly downloaded MODIS LAI image (Table 15).

Based on the relative RMSE, the aerial photo derived LAI map at the 1m spatial resolution had the largest error, then TM derived LAI product at both the 30 m and 250 m spatial resolutions. When the TM images were scaled up to the spatial resolutions of 500 m and 1 km, the relative errors were slightly smaller than those obtained using the MODIS images (Figure 20). Overall, the relative errors varied from 14% to 40%. The relative error (40%) from the aerial photo derived LAI map at local level was relatively large. Both the TM and MODIS derived LAI products had acceptable relative error less than 25% and especially less than 18% at the spatial resolutions of 500 m and 1 km for regional and global level.

Table 15: Descriptive statistic and correlation between the LAI products (estimation maps) obtained using aerial photo, Landsat TM and MODIS images.

STATISTICS OF INDIVIDUAL LAYERS				
Layer	Minimum	Maximum	Mean	Std Deviation
Aerial 1km	4.38	5.45	4.92	0.32
Landsat 1km	2.50	6.49	4.82	1.04
MODIS 1km	2.21	6.22	4.80	0.93
MODIS LAI 1km	12	45	29.88	10.82
COVARIANCE MATRIX				
Layer	Aerial 1km	Landsat 1km	MODIS 1km	MODIS LAI 1km
Aerial 1km	0.10	0.13	0.13	0.62
Landsat 1km	0.13	1.08	0.52	2.37
MODIS 1km	0.13	0.52	0.86	5.31
MODIS LAI 1km	0.62	2.37	5.31	117.11
CORRELATION MATRIX				
Layer	Aerial 1km	Landsat 1km	MODIS 1km	MODIS LAI 1km
Aerial 1km	1	0.38	0.43	0.17
Landsat 1km	0.38	1	0.54	0.21
MODIS 1km	0.43	0.54	1	0.52
MODIS LAI 1km	0.17	0.21	0.52	1

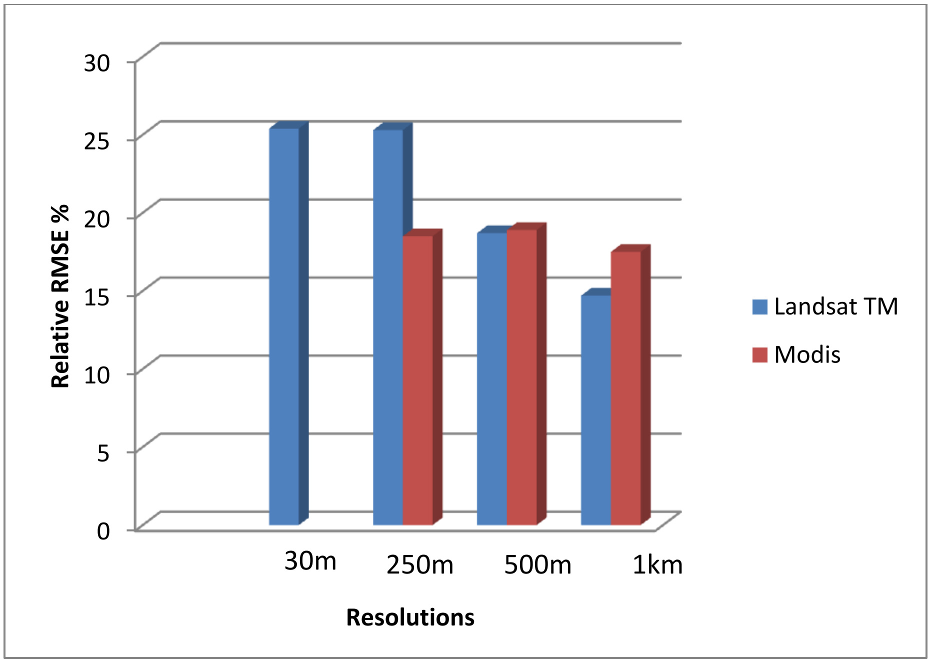

Figure 20: Comparison of Landsat TM and MODIS derived LAI maps based on relative RMSE.

CHAPTER 5
DISCUSSION

5.1 SAMPLING DESIGN AND MAP ACCURACY

The sampling design used in this study was found effective in relation to multiple spatial resolutions for the heterogeneous landscape of Southern Illinois. First of all, the sample plots were evenly distributed over the study area. This has led to consistent sampling at uniform distance which helped to reduce the time to measuring sample plots. Secondly, this sampling design resulted in the sampling distances that matched the spatial resolutions of 1 m, 30 m, 90 m, 250 m, 500 m, and 1 km that are often required to map LAI at local, regional and global scale. Therefore, the obtained LAI observations could easily be combined with the remotely sensed images at various spatial resolutions. These observations could also be used to assess the accuracy of the image derived LAI products; especially the MODIS derived LAI maps. This sampling design provided the potential to obtain and assess LAI products at various spatial resolutions and overcame the gaps that currently existed in this area.

5.2 CORRELATION OF SPECTRAL VARIABLES WITH LAI

Overall, the Landsat TM bands had much higher correlations with LAI than the aerial photo and MODIS and the correlations decreased as the TM images were scaled up from a finer spatial resolution to a coarser one. The similar results were obtained for MODIS images. Band combinations including band ratios, additions, subtractions, and multiplications) often led to higher correlation with LAI than the original channels for all the aerial photo, TM and MODIS images. This was mainly because the band combinations reduced the effects of topographic features (slope and aspect) and atmospheric conditions.

For the TM images, the blue band 1 and two middle infrared bands 5 and 7 and their relevant combinations often led to higher correlation with LAI. On the other hand, the widely used vegetation indices that are associated with red and near infrared bands, including SR, NDVI, and EVI, showed only moderate correlations with LAI. Thus, they were removed from the models by the stepwise regression method. For MODIS images, in terms of correlation with LAI, the best band varied from the band ratio – Blue * Red / NIR at the 250 m spatial resolution to blue band at both the 500 m and 1 km spatial resolution. But, the widely used vegetation indices (SR, NDVI, and EVI) were often involved in the regression models because their moderate correlations with LAI were higher than the other band combinations. The results were consistent with the findings in other studies (Huete et al. 1997; Spanner et al. 1990).

5.3 LAI MAPPING VS IMAGES AT VARIOUS SPATIAL RESOLUTIONS

In this study, LAI maps were generated using the images from high spatial resolution aerial photo to medium resolution Landsat TM images and coarse resolution MODIS images. All the LAI maps perfectly mapped the spatial variability of LAI that matched the land cover types including forests, agricultural lands, grasslands, and shrubs. Larger LAI values dominated this study area because this study area was mainly covered by the hardwood forests. It was found that the forested areas often had LAI values larger than 5, the shrub lands had the values from 4 to 5, the agricultural lands had the values from 2 to 4, and the grass lands had the values less than 2.

Theoretically, high spatial resolution images can be used to accurately produce LAI maps for a given local area. High spatial resolution LAI maps can entail the vegetation covers for a local area (Peellikka et al. 2000; Wulder et al. 2004). However, in this study, the aerial photo derived LAI map that was associated with low correlation between the estimated and observed

LAI values and large relative RMSE had great overestimation for the small LAI observations and large underestimation for the large LAI observations. The main reasons might be because the aerial photo had only three visible bands: blue, green, and red, and thus fewer opportunities to use them to calculate image transformations or band combinations. Therefore, less information can be extracted from these visible bands. The band combinations from these three bands highly duplicated the information. Also, the high spatial resolution aerial photo disintegrates trees canopies (Cohen et al., 1990; Turner et al., 1999) and led to the undesirable pixilated LAI map.

Compared to the high spatial resolution aerial photo, both multi-spectral sensors Landsat TM and MODIS provided images that are more promising to map LAI because the spectral variables from these sensors are capable enough to extract multi-spectral information that entails the vegetation canopies. This finding was consistent with the conclusions of many other studies (Chen et al. 2002; Yang et al. 2007). The TM derived LAI products had acceptable relative errors for the LAI maps at both medium and coarser spatial resolutions and thus the maps were applicable at local and regional scale. The TM derived LAI maps at the spatial resolutions of 30 m, 90 m, 250 m, 500 m, and 1km showed greater potential due to information from visible as well as near and middle infrared bands. Especially, the TM derived LAI map at the 30m spatial resolution showed a distinct range of LAI estimates that matched the LAI observations and captured the areas with high LAI values. The high LAI values suggested the presence of the hardwood forests in this study area. On the other hand, this also implies that the hardwood forests probably are still carbon sinks. In addition, similar results were obtained from the aggregated TM images.

Although the MODIS derived LAI maps had smaller relative errors than the TM derived LAI products, they were less pronounced and showed less spatial details compared to the TM derived LAI map at the 30 m resolution. That is, the MODIS derived LAI maps are acceptable at regional and global scale, but, less potential for their use at local scale. Moreover, the directly downloaded MODIS LAI product was significantly correlated with the MODIS derived LSAI map at the 1 km resolution, but, not significant with the TM derived LAI map at the same resolution. In addition, the spatial distribution of LAI values from the directly downloaded MODIS LAI product looked slightly different from both the TM and MODIS derived LAI maps in this study. This may imply that one should take caution for using the directly downloaded MODIS LAI image.

5.4 ACCURACY ASSESSMENT OF MODELS

In this study, the sampling design could be used to collect LAI measurements for mapping LAI in combination with various spatial resolutions and for conducting accuracy assessment of corresponding products. This overcame the gap that currently exists in the multi-scale image mapping and accuracy assessment. But, in this study, an independent sampling was not carried out for quantifying the quality of the LAI products.

The validation results showed that the aerial photo driven model was not acceptable because of its larger RMSE at a local scale. This was mainly caused by the overestimation for the smaller LAI observations and the underestimation for the larger LAI values. This implied the aerial photo visible bands lacked of the ability to capture the spatial variation of LAI due to different vegetation canopy types especially in the study area that was dominated by the hardwood forests.

In comparison with the models that were driven by the aerial photo and MODIS images, the models driven by the spectral variables from Landsat TM images had better performance in terms of accuracy of estimates and capturing the spatial variability of LAI although slightly underestimation took place. The TM derived LAI map at the 30 m spatial resolution captured more complexity and heterogeneity of vegetation canopy structures over the MODIS derived LAI map and this finding supported the conclusion made by Yang et al. (2007). The TM bands especially bands 1, 5 and 7 and their combinations provided the greater potential as the predictor variables of LAI. The uncertainties of the LAI estimates may be due to modeling error, misregistration of pixels, and mixed pixels (Zarate-Valdez et al. 2012).

Developing LAI products at coarser spatial resolutions has been widely used for regional and global mapping by degrading high spatial resolution images (Fernandes et al. 2003; Wulder et al. 2004). In this study, the degraded TM LAI products were highly correlated with the LAI observations as the MODIS derived LAI products. This implied the medium spatial resolution TM images provided the potential to generate LAI maps at regional and global scale by data aggregation, as suggested by Kauwe et al. (2011).

Moreover, the MODIS driven regression models at the spatial resolution of 250 m, 500 m, and 1 km showed acceptable relative errors. Although the model at the 1 km resolution had a lower relative error, it provided the smoothed LAI estimates and their spatial variability got loss. This implied the coarse spatial resolution LAI products cannot be used at local scales.

5.5 RESEARCH QUESTIONS AND HYPOTHESES REVISITED

This study was able to come up with the rational answers to the research questions posed.

1. What sampling design method is effective to collect measurements of LAI for the heterogeneous landscape in southern Illinois so that the obtained LAI observations can be used to map LAI and validate the accuracy of the maps at different spatial resolutions?

The answer to the first question was associated with the sampling design. The sampling was designed in such a way that it fits multiple spatial resolutions by using variable sampling distances. The systematic sampling protocol for collection of field observations at equal distances in the study area helps to systematically cover the entire study area and further reduce the biasness and cost in field data collection. Secondly, the samples were measured inside a 30 m sample plot where a transect line was drawn with an equal interval of 6 m to allocate five measured locations to collect LAI values. The spatial configuration of the obtained LAI observations matched 1 m and 30 m spatial resolutions. Thirdly, the study area was divided into 1 km blocks that consisted of smaller nested 250 m and 500 m blocks and the 30 m sample plots were then allocated along the diagonal of the blocks. The spatial configuration of the 30 m sample plots thus matched the pixel sizes of MODIS images at the 250 m, 500 m, and 1 km spatial resolutions. The sampling design captured the spatial variability and heterogeneity of vegetation canopy and biomass structures at variable spatial resolutions.

2 How does LAI vary over space depending on different vegetation types and canopy structures, including forests, shrubs and grass lands?

The selected study area was located in the Southern Illinois and dominated by the hardwood forests. But, the shrubs, agricultural lands and grass lands were also scattered over the landscape. In this study, the TM derived LAI maps well reproduced the spatial variation of LAI. Both the aerial photo and MODIS driven models performed poorer work in terms of capturing the spatial variability of the vegetation canopy structures because of pixilated and smoothed results for the aerial photo and MODIS, respectively.

3 Does a MODIS derived LAI maps have significantly lower accuracy and less detail than the Landsat TM derived LAI map?

The answer to the question was confirmed. Although at the 30 m spatial resolution, the TM derived LAI maps captured more details than the MODIS derived LAI maps, the MODIS derived LAI maps were not good as the TM derived LAI maps by aggregating the TM images from a finer spatial resolution to coarser ones: 500 m and 1 km. At the spatial resolution of 250 m, the MODIS derived LAI map had slightly poorer accuracy than the TM derived LAI map. But, the MODIS derived LAI maps were found to have smaller ranges of LAI values compared to the field observations. That is, the MODIS driven models smoothed the LAI values due to coarser spatial resolutions and lacking of the ability to capture the detailed variation of LAI (Cohen et.al 2006).

Moreover, this study proved the hypothesis: statistically, the spectral variables from Landsat TM and MODIS images were significantly correlated with LAI. The correlation varied depending on different bands and their combinations. The best bands were bands 5, 1, and 7 and their relevant combinations for TM images, and red and blue band and their relevant combinations for MODIS images. Overall, the band combinations led to better correlations with LAI than the original channels. The widely used three vegetation indices had moderate correlation with LAI.

There were several limitations in this study. First of all, a classification of land use and land cover types was not conducted. Thus, there was a lack of exploring the spatial variation of LAI estimates within each of vegetation canopy types. Had this LAI mapping been conducted in terms of species richness and land cover types, there would have been more information provided on carbon modeling. Another shortcoming of this study was that the selected study area was too small, which limited the investigation of using MODIS images to map LAI at global scale. Thus, one should take caution to use the conclusions made related to the MODIS images, when a large study area is taken into account.

CHAPTER 6

CONCLUSIONS & RECOMMENDATIONS

As a key biophysical parameter of process based models that are used to predict carbon sequestration of terrestrial ecosystems, LAI plays an important role in the global carbon cycle modeling. Mapping LAI is thus very important in the area of carbon science and management. A substantial research has been conducted. However, many big challenges still exist. This study conducted a pilot study in the complex landscape located in the Southern Illinois to map LAI by combining field observations and remotely sensed images. Multi-scale mapping and accuracy assessment of LAI using various spatial resolution images including aerial photo, Landsat TM and MODIS images were carried out in order to overcome some of the gaps that currently exist in this area. The following conclusions can be drawn from this study.

First of all, a specific sampling design was developed. The results showed that the sampling design could be used to collect LAI observations to create LAI products at various spatial resolutions. The spatial configuration of the LAI observations could match multiple spatial resolutions that varied from 1 m to 30 m, 90 m, 250 m, 500 m, and 1 km. The spatial resolutions are consistent with the pixel sizes of aerial photo, Landsat TM and MODIS images. Moreover, the sampling design was able to capture the spatial variability and patterns of LAI of a heterogeneous landscape. The collected LAI observations could also be used to assess the quality of the multiple spatial resolution LAI maps especially those derived using coarser MODIS image. Thus, this study overcame some of the significant gaps in this area.

Secondly, the TM derived LAI maps successfully characterized the heterogeneous landscape and captured the spatial variability of LAI in this study. The TM derived maps was better than those from the aerial photo and MODIS in terms of the spatial details and accuracy. Thus, the TM images are applicable to map LAI at local, region and global scale.

Moreover, the aerial photo driven model not only over- and under-estimated the LAI values of the sample plots, but also led to a pixilated map of LAI. Thus, it is not applicable even at local scale. The MODIS derived LAI maps had slightly lower accuracy compared to the TM derived LAI maps. In addition, the MODIS derived LAI maps also smoothed the LAI values and lacked of the ability to capture the spatial variability of LAI. The reason might be this study area was not large enough to show the capability of MODIS images at coarser spatial resolutions. That is, one should take caution for use of MODIS images for small areas.

Another finding was that the widely used vegetation indices (SR, NDVI and EVI) did not always have highest correlation with LAI. In terms of the correlation, the best bands varied depending on different sensors. The band combinations often led to higher correlations with LAI than the original bands. This study opened door for further vegetation study of Southern Illinois using multiple sensors by enlarging study area and design at broader scale. Future studies could be done on specific plant communities of oak-hickory species and agricultural crops to assess Leaf Area Index and spatial distribution patterns in Southern Illinois.

6.1 LIMITATIONS OF THIS STUDY

There were a couple of shortcomings in this research. Firstly, the used Landsat TM images were not consistent with the LAI field observations in time. When the LAI field measurements were collected in the summer of 2012, there were no Landsat TM images available. Secondly, the used aerial photo was dated in 2007. We assumed that in this study area land use and land cover types were relatively stable and no significant changes took place except vegetation growing.

REFERENCES

Braun, Emma Lucy. 1950. "Deciduous forests of eastern North America." *Deciduous forests of Eastern North America*.

Bréda, Nathalie J J. 2003. “Ground-based Measurements of Leaf Area Index: a Review of Methods, Instruments and Current Controversies.” *Journal of Experimental Botany* 54 (392) (November): 2403–17. doi:10.1093/jxb/erg263.

Busetto, L, M Meroni, and R Colombo. 2008. “Combining Medium and Coarse Spatial Resolution Satellite Data to Improve the Estimation of Sub-pixel NDVI Time Series.” *Remote Sensing of Environment* 112 (1) (January 15): 118–131. doi:10.1016/j.rse.2007.04.004.

Campbell, G.S. 1986. “Extincition coefficients for radiation in plant canopies calculated using an ellipsoidal inclination angle distribution”. *Agricultural and Forest Meteorology*, 36(4): 317-321

Chen, J.M, G Pavlic, L Brown, J Cihlar, S.G Leblanc, H.P White, R.J Hall, et al. 2002. “Derivation and Validation of Canada-wide Coarse-resolution Leaf Area Index Maps Using High-resolution Satellite Imagery and Ground Measurements.” *Remote Sensing of Environment* 80 (1) (April): 165–184. doi:10.1016/S0034-4257(01)00300-5.

Chen, Jing M., and T. A. Black. "Defining leaf area index for non-flat leaves." *Plant, Cell & Environment* 15, no. 4 (1992): 421-429.

Chen, Jing M., and Josef Cihlar. 1996. "Retrieving leaf area index of boreal conifer forests using Landsat TM images." *Remote sensing of environment* 55, no. 2: 153-162.

Chen, J.M., C.H. Menges, and S.G. Leblanc. 2005. “Global Mapping of Foliage Clumping Index Using Multi-angular Satellite Data.” *Remote Sensing of Environment* 97 (4) (September): 447–457. doi:10.1016/j.rse.2005.05.003.

Chen, Jing M., Paul M. Rich, Stith T. Gower, John M. Norman, and Steven Plummer. 1997. “Leaf Area Index of Boreal Forests: Theory, Techniques, and Measurements.” *Journal of Geophysical Research* 102 (D24) (December 1): 29429. doi:10.1029/97JD01107.

Chen, Jing M. Remote Sensing of Leaf Area Index of Vegetation Covers. 2013. Spatial uncertainty analysis when mapping natural resources using remotely sensed data. In G. Wang, and Q. Weng (Eds.) *Remote Sensing of Natural Resources.* CRC Press, Taylor & Francis Group. Pp: 375-398.

Cohen, Warren B., Thomas A. Spies, and Gay A. Bradshaw. 1990. "Semivariograms of digital imagery for analysis of conifer canopy structure." *Remote Sensing of Environment* 34, no. 3: 167-178.

Cohen, W.B., T.K. Maiersperger, D.P. Turner, W.D. Ritts, D. Pflugmacher, R.E. Kennedy, a. Kirschbaum, S.W. Running, M. Costa, and S.T. Gower. 2006a. "MODIS Land Cover and LAI Collection 4 Product Quality Across Nine Sites in the Western Hemisphere." *IEEE Transactions on Geoscience and Remote Sensing* 44 (7) (July): 1843–1857. doi:10.1109/TGRS.2006.876026.

Cohen, W. B, Thomas K Maiersperger, Zhiqiang Yang, Stith T Gower, David P Turner, William D Ritts, Mercedes Berterretche, and Steven W Running. 2003. "Comparisons of Land Cover and LAI Estimates Derived from ETM+ and MODIS for Four Sites in North America: a Quality Assessment of 2000/2001 Provisional MODIS Products." *Remote Sensing of Environment* 88 (3) (December): 233–255. doi:10.1016/j.rse.2003.06.006.

Congalton, R. G., and K. Green. 2009. *Assessing the accuracy of remotely sensed data: principles and practices*. 2nd ed. FL: CRC Press.

Congalton, R.G. 1991. A review of assessing the accuracy of classifications of remotely sensed data. *Remote Sensing of Environment* 37: 35–46.

De Kauwe, M.G., M.I. Disney, T. Quaife, P. Lewis, and M. Williams. 2011. "An Assessment of the MODIS Collection 5 Leaf Area Index Product for a Region of Mixed Coniferous Forest." *Remote Sensing of Environment* 115 (2) (February 15): 767–780. doi:10.1016/j.rse.2010.11.004.

Doraiswamy, P.C., J.L. Hatfield, T.J. Jackson, B. Akhmedov, J. Prueger, and A. Stern. 2004. "Crop Condition and Yield Simulations Using Landsat and MODIS." 2002 Soil Moisture Experiment (SMEX02) 92 (4) (September 30): 548–559. doi:10.1016/j.rse.2004.05.017.

Eklundh, Lars, Lars Harrie, and Andres Kuusk. 2001. "Investigating Relationships Between Landsat ETM+ Sensor Data and Leaf Area Index in a Boreal Conifer Forest." *Remote Sensing of Environment* 78 (3) (December): 239–251. doi:10.1016/S0034-4257(01)00222-X. http://linkinghub.elsevier.com/retrieve/pii/S003442570100222X.

Fernandes, Richard, Chris Butson, Sylvain Leblanc, and Rasim Latifovic. 2003. "Landsat-5 TM and Landsat-7 ETM+ Based Accuracy Assessment of Leaf Area Index Products for Canada Derived from SPOT-4 VEGETATION Data." *Canadian Journal of Remote Sensing* 29 (2) (April): 241–258. doi:10.5589/m02-092. http://pubs.casi.ca/doi/abs/10.5589/m02-092.

Fralish, James S. 2003. "The central hardwood forest: its boundaries and physiographic provinces." *UNITED STATES DEPARTMENT OF AGRICULTURE FOREST SERVICE GENERAL TECHNICAL REPORT NC* : 1-20.

Friedl, M. A., D. S. Schimel, J. Michaelsen, F. W. Davis, and H. Walker. "Estimating grassland biomass and leaf area index using ground and satellite data. 1994. *"International Journal of Remote Sensing* 15, no. 7: 1401-1420.

Ganguly, Sangram, Arindam Samanta, Mitchell A. Schull, Nikolay V. Shabanov, Cristina Milesi, Ramakrishna R. Nemani, Yuri Knyazikhin, and Ranga B. Myneni. 2008. "Generating vegetation leaf area index Earth system data record from multiple sensors. Part 2: Implementation, analysis and validation." *Remote Sensing of Environment* 112, no. 12: 4318-4332.

Gobron, Nadine, Bernard Pinty, and Michel M. Verstraete. 1997. "Theoretical limits to the estimation of the leaf area index on the basis of visible and near-infrared remote sensing data." *Geoscience and Remote Sensing, IEEE Transactions on* 35, no. 6: 1438-1445.

Goetz, S. J. 1997. "Multi-sensor Analysis of NDVI, Surface Temperature and Biophysical Variables at a Mixed Grassland Site." *International Journal of Remote Sensing* 18 (1) (January 1): 71–94. doi:10.1080/014311697219286.

Gray, Josh, and Conghe Song. 2012. "Mapping Leaf Area Index Using Spatial, Spectral, and Temporal Information from Multiple Sensors." *Remote Sensing of Environment* 119 (April): 173–183. doi:10.1016/j.rse.2011.12.016.

Hassan, Quazi K., and Charles P.-a. Bourque. 2010. "Spatial Enhancement of MODIS-based Images of Leaf Area Index: Application to the Boreal Forest Region of Northern Alberta, Canada." *Remote Sensing* 2 (1) (January 8): 278–289. doi:10.3390/rs2010278.

Hosner, John F., and Leon S. Minckler. 1963. "Bottomland hardwood forests of southern Illinois--regeneration and succession." *Ecology* 44, no. 1: 29-41.

Huang, Dong, Wenze Yang, Bin Tan, Miina Rautiainen, Ping Zhang, Jiannan Hu, Nikolay V. Shabanov, Sune Linder, Yuri Knyazikhin, and Ranga B. Myneni. 2006. "The importance of measurement errors for deriving accurate reference leaf area index maps for validation of moderate-resolution satellite LAI products." *Geoscience and Remote Sensing, IEEE Transactions on* 44, no. 7: 1866-1871.

Huete, A, K Didan, T Miura, E.P Rodriguez, X Gao, and L.G Ferreira. 2002. "Overview of the Radiometric and Biophysical Performance of the MODIS Vegetation Indices." *Remote Sensing of Environment* 83 (1-2) (November): 195–213. doi:10.1016/S0034-4257(02)00096-2.

Huete, A.R., H.Q. Liu, K. Batchily, and W. van Leeuwen. 1997. "A Comparison of Vegetation Indices over a Global Set of TM Images for EOS-MODIS." *Remote Sensing of Environment* 59 (3) (March): 440–451. doi:10.1016/S0034-4257(96)00112-5.

Illinois Department of Natural Resources. Illinois Trees Forest Facts: 2008. http://dnr.state.il.us/education/classrm/treeseedsleaves/treefacts.htm

Jensen, Ryan R., and Perry J. Hardin. 2005. “Estimating Urban Leaf Area Using Field Measurements and Satellite Remote Sensing Data.” *Journal of Arboriculture* 31 (1): 21–27.

Jonckheere, Inge, Stefan Fleck, Kris Nackaerts, Bart Muys, Pol Coppin, Marie Weiss, and Frédéric Baret. 2004. "Review of methods for in situ leaf area index determination: Part I. Theories, sensors and hemispherical photography." *Agricultural and forest meteorology* 121, no. 1: 19-35.

Luyssaert, Sebastiaan, E-Detlef Schulze, Annett Börner, Alexander Knohl, Dominik Hessenmöller, Beverly E Law, Philippe Ciais, and John Grace. 2008. “Old-growth Forests as Global Carbon Sinks.” *Nature* 455 (7210) (September 11): 213–5. doi:10.1038/nature07276.

Myneni, R. B., S. Hoffman, Yu Knyazikhin, J. L. Privette, J. Glassy, Y. Tian, Y. Wang, X. Song, Y. Zhang, and G. R. Smith. 2002. “Global Products of Vegetation Leaf Area and Fraction Absorbed PAR from Year One of MODIS Data.” *Remote Sensing of Environment* 83 (1): 214–231.

Pande, A., Carol L. Williams, C.L.Lant, and D.J.Gibson. 2007. “Using map algebra to determine the mesoscale distribution of invasive plants: the case of *Celastrus orbiculatus* in Southern Illinois, USA.” Biol Invasions (9):419 - 431

Peduzzi, Alicia, Randolph H. Wynne, Thomas R. Fox, Ross F. Nelson, and Valerie a. Thomas. 2012. “Estimating Leaf Area Index in Intensively Managed Pine Plantations Using Airborne Laser Scanner Data.” *Forest Ecology and Management* 270 (April): 54–65. doi:10.1016/j.foreco.2011.12.048.

Pfeifer, Marion, Alemu Gonsamo, Mathias Disney, Petri Pellikka, and Rob Marchant. 2012. “Leaf Area Index for Biomes of the Eastern Arc Mountains: Landsat and SPOT Observations Along Precipitation and Altitude Gradients.” *Remote Sensing of Environment* 118 (March): 103–115. doi:10.1016/j.rse.2011.11.009.

Pregitzer, Kurt S., and Eugenie S. Euskirchen. 2004. “Carbon Cycling and Storage in World Forests: Biome Patterns Related to Forest Age.” *Global Change Biology* 10 (12) (December): 2052–2077. doi:10.1111/j.1365-2486.2004.00866.x.

Qi, J., Y. H. Kerr, M. S. Moran, M. Weltz, A. R. Huete, S. Sorooshian, and R. Bryant. 2000. “Leaf Area Index Estimates Using Remotely Sensed Data and BRDF Models in a Semiarid Region.” *Remote Sensing of Environment* 73 (1): 18–30.

Ross, J. 1981. “The radiation regime and architecture of plant stands” Dr. W. Junk Publishers pp.391

Rouse, J.W., R.H. Hass, J.A. Scheel, D.W.Deering, and J.C. Harlan. 1974. “Monitoring the vernal advancement of regrogradation of natural vegetation, NASA/GSFC, Type III, Final Report, Greenbelt, MD, USA, pp 1-371.

Running, Steven W., R.R. Nemani, D.L. Peterson, L.E.Band, D.F. Potts, L.L. Pierce, and M.A. Spanner. 1989. “Mapping Regional Forest Evapotranspiration and photosynthesis by Coupling Satellite Data with Ecosystem Simulation,” *Ecology*, 70(4): 1090-1101

Running, Steven W., and Stith T. Gower. 1991. “FOREST-BGC, A General Model of Forest Ecosystem Processes for Regional Applications. II. Dynamic Carbon Allocation and Nitrogen Budgets.” *Tree Physiology* 9 (1_2): 147–160.

Running, Steven W., and E. Raymond Hunt. 1993. "Generalization of a forest ecosystem process model for other biomes, BIOME-BGC, and an application for global-scale models." *Scaling physiological processes: Leaf to globe*: 141-158.

Sellers, Piers J., Compton J. Tucker, G. James Collatz, Sietse O. Los, Christopher O. Justice, Donald A. Dazlich, and David A. Randall. 1996. “A Revised Land Surface Parameterization (SiB2) for Atmospheric GCMS. Part II: The Generation of Global Fields of Terrestrial Biophysical Parameters from Satellite Data.” *Journal of Climate* 9 (4) (April 1): 706–737. doi:10.1175/1520-0442(1996)009<0706:ARLSPF>2.0.CO;2.

Schiffman, Bettina, Galli Basson, Evan Lue, Dustin Ottman, Anjanette Hawk, Moyukh Ghosh, Forrest Melton, Cindy Schmidt, and J. W. Skiles. "ESTIMATION OF LEAF AREA INDEX (LAI) THROUGH THE ACQUISITION OF GROUND TRUTH DATA IN YOSEMITE NATIONAL PARK." ASPRS 2008 Annual Conference, Portland, Oregon, April 28 – May 2, 2008

Spanner, Michael A., Lars L. Pierce, David L. Peterson, and Steven W. Running. 1990. "Remote sensing of temperate coniferous forest leaf area index The influence of canopy closure, understory vegetation and background reflectance." *Title REMOTE SENSING* 11, no. 1: 95-111.

Thompson, Frank R. “The Hoosier- Shawnee Ecological.”

Turner, David P., Warren B. Cohen, Robert E. Kennedy, Karin S. Fassnacht, and John M. Briggs. 1999. “Relationships Between Leaf Area Index and Landsat TM Spectral Vegetation Indices Across Three Temperate Zone Sites.” *Remote Sensing of Environment* 70 (1): 52–68.

Turner, D. P., S. Ollinger, M-L. Smith, O. Krankina, and M. Gregory. 2004. "Scaling net primary production to a MODIS footprint in support of Earth observing system product validation." *International Journal of Remote Sensing* 25, no. 10: 1961-1979.

Viña, Andrés, Anatoly a. Gitelson, Anthony L. Nguy-Robertson, and Yi Peng. 2011. “Comparison of Different Vegetation Indices for the Remote Assessment of Green Leaf Area Index of Crops.” *Remote Sensing of Environment* 115 (12) (December): 3468–3478. doi:10.1016/j.rse.2011.08.010.

www.netstate.com/states/geography/ il_geography.htm

Watson, D.J. 1947. “Comparative physiological studies in the growth of field crops. I: Variation in net assimilation rate and leaf area between species and varieties, and within and between years.” *Annals of Botany*, 31-43

Wang, G., G.Z. Gertner, S. Fang, and A.B. Anderson. 2005. A methodology for spatial uncertainty analysis of remote sensing products. *Photogrammetric Engineering and Remote Sensing* 71: 1423-1432.

Wang, G., T. Oyana, M. Zhang, S. Adu-Prah, S. Zeng, H. Lin, and J. Se. 2009. Mapping and spatial uncertainty analysis of forest vegetation carbon by combining national forest inventory data and satellite images. *Forest Ecology and Management* 258(7):1275-1283.

Wang, G., G.Z. Gertner. 2013. Spatial uncertainty analysis when mapping natural resources using remotely sensed data. In G. Wang, and Q. Weng (Eds.) *Remote Sensing of Natural Resources*. CRC Press, Taylor & Francis Group, P: 87-107.

Wang, Y., Curtis E. Woodcock, Wolfgang Buermann, Pauline Stenberg, Pekka Voipio, Heikki Smolander, T. Hame, Yuhong Tian, Jiannan Hu, and Yuri Knyazikhin. 2003. “Validation of the MODIS LAI Product in Coniferous Forest of Ruokolahti, Finland.” *Remote Sens. Environ*. 410–455.

Woodcock, Curtis E., and Alan H. Strahler. 1987. "The factor of scale in remote sensing." *Remote sensing of Environment* 21, no. 3: 311-332.

Wulder, Michael A., Ronald J. Hall, Nicholas C. Coops, and Steven E. Franklin. 2004. “High Spatial Resolution Remotely Sensed Data for Ecosystem Characterization.” *BioScience* 54 (6): 511–521.

Xavier, Alexandre Cândido, and Carlos Alberto Vettorazzi. 2004. “Monitoring Leaf Area Index at Watershed Level through NDVI from Landsat-7/ETM+ Data.” *Scientia Agricola* 61 (3): 243–252.

Yang, Peng, Ryosuke Shibasaki, Wenbin Wu, Qingbo Zhou, Zhongxin Chen, Yan Zha, Yun Shi, and Huajun Tang. 2007. "Evaluation of MODIS land cover and LAI products in cropland of North China Plain using in situ measurements and Landsat TM images." *IEEE Transactions on Geoscience and Remote Sensing* 45, no. 10.

Yates, Emily D., D. F. Levia Jr., and Carol L. Williams. 2004. “Recruitment of three non-native invasive plants into a fragmented forest in southern Illinois” *Forest Ecology and Management* 190 (November): 119-130

Zarate-Valdez, Jose L., Michael L. Whiting, Bruce D. Lampinen, Samuel Metcalf, Susan L. Ustin, and Patrick H. Brown. 2012. “Prediction of Leaf Area Index in Almonds by Vegetation Indexes.” *Computers and Electronics in Agriculture* 85 (July): 24–32. doi:10.1016/j.compag.2012.03.009.

Zha, Yong, Jay Gao, Shaoxiang Ni, Yansui Liu, Jianjun Jiang, and Yuchun Wei. 2003. "A Spectral Reflectance-based Approach to Quantification of Grassland Cover from Landsat TM Imagery." *Remote Sensing of Environment* 87 (2-3) (October): 371–375. doi:10.1016/j.rse.2003.05.001.

Zheng, Guang, and L Monika Moskal. 2009. "Retrieving Leaf Area Index (LAI) Using Remote Sensing: Theories, Methods and Sensors." *Sensors (Basel, Switzerland)* 9 (4) (January): 2719–45. doi:10.3390/s90402719.

APPENDIX

Appendix A

PlotID	x	y	LAI1	LAI2	LAI3	LAI4	LAI5	COVER TYPES	LAI 30m	LAI 250m	LAI 500m	LAI 1km
1	302562.5	4163843	6.06	6.39	6.62	6.46	6.66	moderate forest	6.44			
2	302750	4164030	6.38	6.19	6.32	6.16	6.11	moderate forest	6.23			
3	302875	4164155	0.05	0.08	1.42	5.95	5.08	bare soil/grass/shrubs	2.52			
4	302937.5	4164218	3.02	1.09	3.21	5.22	4.44	grass/shrubs	3.40	2.38	3.91	4.59
5	303000	4164280	1.05	1.47	1.35	1.21	1.04	grass	1.22			
6	303125	4164405	5.25	5.69	6	6.52	7.54	moderate forest	6.20			
7	303312.5	4164530	6.69	5.45	6.3	6.6	5.54	moderate forest	6.12			
1	302562.5	4162843	4.03	3.43	3.74	3.88	4.27	shrubs area/few tree stands	3.87			
2	302750	4163030	4.96	5.27	5.37	3.72	5.86	few tree stands	5.04			
3	302875	4163155	5.71	6.35	6.2	6.23	6.16	moderate forest	6.13			
4	302937.5	4163218	6.32	6.34	6.18	6.24	2.49	moderate forest	5.51	5.71	5.65	5.35
5	303000	4163280	4.76	5.19	5.52	5.8	6.13	sparse forest cover	5.48			
6	303125	4163405	6.03	6.07	6.19	6.11	6.14	moderate forest	6.11			

7	303312.5	4163530	5.12	4.68	5.61	5.87	5.17	sparse forest cover/swampy area	5.29			
1	303562.5	4163843	4.89	4.6	5.08	4.49	5.13	sparse forest cover	4.84			
2	303750	4164030	5.02	6.05	5.99	6.11	6.13	moderate forest cover	5.86			
3	303875	4164155	3.72	4.18	4.32	5.75	7.35	sparse forest cover	5.06			
4	303937.5	4164218	6.46	6.31	6.02	6.33	5.83	moderate forest cover	6.19	5.85	6.06	5.92
5	304000	4164280	5.57	6.5	8.4	5.9	5.13	sparse forest cover	6.30			
6	304125	4164405	7.02	6.9	6.87	6.92	6.84	dense forest cover	6.91			
7	304312.5	4164530	6.85	7.5	6.5	5.5	5.1	moderate forest cover	6.29			

1	302562.5	4161843	0.02	0.04	0.2	0.5	0.3	grass/strawfield	0.21			
2	302750	4162030	2.73	2.62	1.75	1.89	2.16	grass	2.23			
3	302875	4162155	0.29	0.31	0.45	0.42	0.38	grass	0.37			
4	302937.5	4162218	1.07	0.92	0.88	0.81	0.81	grass	0.90	0.61	1.38	1.51
5	303000	4162280	0.56	0.65	0.54	0.51	0.57	grass	0.57			
6	303125	4162405	3.6	2.97	2.55	2.57	2.47	shrubs	2.83			
7	303312.5	4162530	2.96	4.14	2.87	3.25	4.15	shrubs	3.47			
1	303562.5	4162843	5.21	5.41	5.61	5.6	5.76	few tree stands	5.52			
2	303750	4163030	1.05	1.62	1.55	1.49	1.2	grassland	1.38			
3	303875	4163155	3.6	3.76	3.32	4.8	3.9	marshy area/shrubs	3.88			
4	303937.5	4163218	5.04	4.87	4.89	4.53	4.62	grass/bushes	4.79	4.28	3.90	4.49
5	304000	4163280	4.47	3.83	4.42	4.09	4.04	swampy area	4.17			
6	304125	4163405	3.96	5.38	5.51	5.85	5.74	swampy area	5.29			
7	304312.5	4163530	6.52	6.6	6.32	6.3	6.27	moderate forest canopy	6.40			

1	304562.5	4163843	7.49	7.46	6.73	6.71	6.92	high forest canopy	7.06			
2	304750	4164030	0.34	0.81	0.52	0.9	1.2	bare land	0.75			
3	304875	4164155	6.85	7.04	7.09	7.14	6.35	mixed pine forest	6.89			
4	304937.5	4164218	5.08	6.14	5.05	5.25	5.21	mixed pine forest	5.35	5.80	4.70	5.16
5	305000	4164280	4.09	4.86	5.32	5.58	5.91	mixed pine forest	5.15			
6	305125	4164405	5.64	5.19	5.68	5.08	5.23	mixed pine forest	5.36			
7	305312.5	4164530	4.23	5.31	5.88	6.18	6.28	mixed pine forest	5.58			
1	302562.5	4160843	0.76	2.56	3.14	4.14	5.63	bare land/grass/shrubs	3.25			
2	302750	4161030	4.11	4.79	5.03	5.23	5.46	forest	4.92			
3	302875	4161155	0.31	0.38	0.29	0.62	0.41	grassland	0.40			
4	302937.5	4161218	6.46	6.89	7.01	7.05	7.1	dense forest	6.90	4.03	4.56	4.57
5	303000	4161280	4.08	4.31	4.76	5.18	5.67	sparse forest canopy	4.80			
6	303125	4161405	5.92	4.7	5.65	6.21	6.27	sparse forest canopy	5.75			
7	303312.5	4161530	4.08	5.64	6.1	6.89	7.21	dense canopy	5.98			
1	303562.5	4161843	6.73	6.56	5.31	7.62	7.39	moderate forest canopy	6.72			

2	303750	4162030	6.59	7.47	6.81	7.52	6.79	high forest canopy	7.04			
3	303875	4162155	5.96	5.82	6.48	6.68	6.42	moderate forest	6.27			
4	303937.5	4162218	4.61	4.83	4.07	5.71	5.32	sparse forest canopy	4.91	5.83	6.46	6.55
5	304000	4162280	5.62	6.45	6.08	6.51	6.82	moderate forest	6.30			
6	304125	4162405	7.81	8.03	8.23	7.56	7.32	high forest canopy	7.79			
7	304312.5	4162530	6.21	6.33	6.76	7.23	7.71	high forest canopy	6.85			
1	304562.5	4162843	5.89	6.76	6.57	7.06	7.17	high forest canopy	6.69			
2	304750	4163030	6.73	6.89	7.86	8.35	8.61	high forest canopy	7.69			
3	304875	4163155	7.12	6.35	6.74	6.63	6.59	moderate forest	6.69			
4	304937.5	4163218	6.46	6.72	7.24	7.05	7.18	high forest canopy	6.93	6.78	7.03	6.89
5	305000	4163280	7.02	6.87	6.45	6.65	6.68	moderate forest canopy	6.73			
6	305125	4163405	7.46	7.34	7.53	6.91	6.29	high forest canopy	7.11			
7	305312.5	4163530	6.56	5.98	6.62	6.58	6.23	moderate forest canopy	6.39			
1	305562.5	4163843	6.71	6.54	6.81	6.63	6.49	moderate forest	6.64			

								canopy				
2	305750	4164030	4.99	4.82	4.79	4.53	4.78	tall grasses	4.78			
3	305875	4164155	5.84	5.63	6.1	6.13	5.96	sparse forest canopy	5.93			
4	305937.5	4164218	5.22	5.25	5.22	5.26	5.4	sparse forest canopy	5.27	5.59	5.28	5.59
5	306000	4164280	5.53	5.32	5.66	5.82	5.56	sparse forest canopy	5.58			
6	306125	4164405	4.63	4.42	4.74	5.11	5.38	sparse forest canopy	4.86			
7	306312.5	4164530	5.16	6.24	6.88	6.51	5.69	moderate forest canopy	6.10			
1	302562.5	4159843	0.23	0.18	0.16	0.21	0.31	empty land	0.22			
2	302750	4160030	4.12	5.86	5.79	6.13	6.5	shrubs/trees	5.68			
3	302875	4160155	3.24	3.61	4.07	4.59	4.47	cornfield	4.00			
4	302937.5	4160218	3.55	2.89	3.01	3.44	3.52	cornfield	3.28	3.12	3.55	3.07
5	303000	4160280	2.85	1.21	2.04	2.02	2.27	grass	2.08			
6	303125	4160405	1.78	2.71	2.01	3.77	3.32	grass/shrubs	2.72			
7	303312.5	4160593	3.4	4.21	3.33	3.46	3.17	cornfield	3.51			
1	303562.5	4160843	4.87	4.92	5.18	5.47	5.39	sparse forest canopy	5.17			

2	303750	4161030	5.31	5.64	6.03	6.15	6.32	sparse forest canopy	5.89			
3	303875	4161155	6.17	6.09	5.81	5.94	6.34	sparse forest canopy	6.07			
4	303937.5	4161218	5.05	4.41	4.72	5.91	6.07	bushes/trees	5.23	5.26	5.59	5.65
5	304000	4161280	3.8	4.25	4.63	4.71	5.02	grasses/bushes	4.48			
6	304125	4161405	5.81	6.05	6.23	6.56	6.72	moderate forest canopy	6.27			
7	304312.5	4161530	6.02	6.24	6.38	6.62	6.81	moderate forest canopy	6.41			
1	304562.5	4161843	5.07	5.25	6.31	5.82	6.45	moderate forest canopy	5.78			
2	304750	4162030	6.06	6.48	6.79	7.03	6.73	moderate forest canopy	6.62			
3	304875	4162155	1.06	1.18	1.03	1.2	1.46	grassland	1.19			
4	304937.5	4162218	4.55	4.71	5.02	5.31	6.26	tall grass/few trees	5.17	4.33	5.16	5.39
5	305000	4162280	6.55	6.59	6.71	6.6	6.74	moderate forest canopy	6.64			
6	305125	4162405	6.43	5.81	6.04	5.77	6.92	moderate forest canopy	6.19			
7	305312.5	4162530	5.67	5.93	6.21	6.64	6.42	sparse forest canopy	6.17			

1	305562.5	4162843	1.25	2.31	1.67	1.34	1.47	grassland	1.61				
2	305750	4163030	5.67	5.94	6.35	6.7	6.56	sparse forest canopy	6.24				
3	305875	4163155	5.39	4.8	5.73	6.46	6.72	sparse forest canopy	5.82				
4	305937.5	4163218	6.74	6.83	7.34	7.58	7.03	high forest canopy	7.10	6.61	6.68	5.89	
5	306000	4163280	7.2	6.81	6.55	6.67	7.31	high forest canopy	6.91				
6	306125	4163405	6.97	7.35	7.08	7.48	7.7	high forest canopy	7.32				
7	306312.5	4163530	6.56	6.47	5.83	6.6	5.59	sparse forest canopy	6.21				
1	306562.5	4163843	5.88	6.16	5.4	5.77	5.8	sparse forest	5.80				
2	306750	4164030	3.51	4.98	3.51	0.61	3.57	sparse forest/open land	3.24				
3	306875	4164155	5.25	5.21	0.3	3.86	3.83	sparse forest/open land	3.69				
4	306937.5	4164218	5.41	4.82	3.72	4.27	4.76	sparse forest	4.60	3.94	3.35	3.65	
5	307000	4164280	3.38	3.06	4.12	3.49	3.67	trees/shrubs	3.54				
6	307125	4164405	1.38	2.13	1.92	1.68	1.35	grass	1.69				
7	307312.5	4164530	1.65	2.34	3.41	3.47	4.05	grass/trees	2.98				

1	303562.5	4159843	2.51	3.2	2.77	2.89	2.75	cornfield	2.82			
2	303750	4160030	5.21	5.07	5.34	3.12	3.29	cornfield/trees	4.41			
3	303875	4160155	4.12	3.28	4.75	5.08	4.68	sparse trees/shrubs	4.38			
4	303937.5	4160218	5.12	5.06	6.07	5.44	5.23	sparse trees/shrubs	5.38	5.10	5.19	4.98
5	303000	4160280	4.88	5.36	5.71	6.11	5.61	forest	5.53			
6	304125	4160405	5.84	6.23	5.78	6.56	6.7	forest	6.22			
7	304312.5	4160593	5.77	6.46	5.82	6.21	6.43	forest	6.14			
1	304562.5	4160843	3.51	3.48	3.27	5.5	5.11	tall grass	4.17			
2	304750	4161030	4.42	4.76	5.24	5.55	5.18	tall grass	5.03			
3	304875	4161155	6.03	6.34	6.57	5.84	6.61	moderate forest canopy	6.28			
4	304937.5	4161218	6.33	5.88	5.46	6.19	6.43	moderate forest canopy	6.06	6.06	5.62	4.66
5	305000	4161280	5.69	6.22	6.12	5.41	5.77	sparse forest canopy	5.84			
6	305125	4161405	5.32	4.6	4.28	5.09	5.21	sparse forest canopy	4.90			
7	305312.5	4161530	0.3	0.37	0.41	0.33	0.41	grass land	0.36			

1	305562.5	4161843	4.9	4.33	0	0.02	0.1	bushes/bare soil	1.87			
2	305750	4162030	1.26	1.12	1.37	1.18	1.27	grass land	1.24			
3	305875	4162155	5.12	5.53	5.78	6.12	6.38	sparse forest	5.79			
4	305937.5	4162218	5.4	4.86	4.78	5.58	5.63	sparse forest	5.25	5.44	4.61	3.90
5	306000	4162280	4.67	4.92	5.33	5.87	5.61	sparse forest	5.28			
6	306125	4162405	5.84	5.43	5.66	5.17	5.34	sparse forest	5.49			
7	306312.5	4162530	3.1	2.2	2.27	2.09	2.31	tall grass	2.39			
1	306562.5	4162843	5.78	5.53	6.21	6.75	6.46	moderate forest	6.15			
2	306750	4163030	6.07	5.48	6.68	6.34	5.7	moderate forest	6.05			
3	306875	4163155	5.48	5.32	5.43	5.12	4.91	mixed pine	5.25			
4	306937.5	4163218	6.4	5.75	5.51	5.8	5.66	mixed pine	5.82	5.44	5.88	5.82
5	307000	4163280	4.6	5.14	5.24	5.86	5.4	sparse forest	5.25			
6	307125	4163405	7.39	7.12	6.97	6.85	6.79	high forest area	7.02			
7	307312.5	4163530	6.17	5.71	4.79	4.13	5.13	sparse forest	5.19			
1	304562.5	4159843	2.37	2.95	2.96	4.62	4.16	grass	3.41			

2	304750	4160030	5.12	4.68	5.89	6.24	5.5	sparse forest	5.49			
3	304875	4160155	6.22	5.64	6.31	6.26	5.8	moderate forest	6.05			
4	304937.5	4160218	5.64	6.36	6.59	5.77	6.05	moderate forest	6.08	5.84	5.83	5.50
5	305000	4160280	5.67	4.89	4.56	5.56	6.21	sparse forest	5.38			
6	305125	4160405	6.43	6.51	6.23	5.63	6.11	moderate forest	6.18			
7	305312.5	4160593	5.86	5.43	6.1	6.45	5.89	sparse forest	5.95			
1	305562.5	4160843	6.3	6.41	6.35	6.59	6.28	forest	6.39			
2	305750	4161030	1.34	1.06	1.44	1.47	1.29	grass	1.32			
3	305875	416115	3.67	4.5	5.44	2.11	4.6	shrubs/grass	4.06			
4	305937.5	4161218	2.55	1.06	0.89	1.11	0.76	grass	1.27	2.13	2.83	3.77
5	306000	4161280	0.66	1.22	1.25	1.08	1.04	grass	1.05			
6	306125	4161405	6.44	5.86	6.75	6.46	6.6	forest	6.42			
7	306312.5	4161530	5.58	5.77	6.35	5.49	6.07	forest/tall grasses	5.85			
1	306562.5	4161843	6.78	6.92	7.23	7.4	6.8	dense forest canopy	7.03			
2	306750	4162030	6.22	6.38	5.88	6.07	6.31	sparse forest	6.17			

3	306875	4162155	6.34	5.69	4.33	2.01	2.44	sparse forest/grass	4.16			
4	306937.5	4162218	1.26	1.04	0.61	0.28	0.06	grass	0.65	3.42	4.60	5.17
5	307000	4162280	5.9	5.44	6.21	4.56	5.2	few trees/shrubs	5.46			
6	307125	4162405	6.71	6.52	6.39	6.8	6.28	few trees/shrubs	6.54			
7	307312.5	4162530	6.37	6.08	6.41	5.67	6.2	moderate forest canopy	6.15			
1	305562.5	4159843	6.94	6.12	6.95	6.84	6.63	sparse canopy	6.70			
2	305750	4160030	7.06	7.13	7.15	7.2	7.03	dense forest cover	7.11			
3	305875	4160155	7.52	7.67	7.68	7.65	8.26	dense forest cover	7.76			
4	305937.5	4160218	4.2	5.25	5.81	6.15	6.33	bushes, dense shrubs	5.55	6.68	6.83	6.65
5	306000	4160280	6.45	6.62	6.75	6.89	6.98	forest cover	6.74			
6	306125	4160405	7.16	7.02	6.98	6.9	6.82	gorge, sloppy area forest	6.98			
7	306312.5	4160593	6.37	5.7	5.19	5.67	5.84	sloppy area	5.75			
1	306562.5	4160843	7.88	7.25	7.22	6.59	6.6	high forest canopy	7.11			
2	306750	4161030	5.41	5.22	4.66	4.7	4.86	tall grass	4.97			

3	306875	4161155	6.07	6.01	6.26	6.23	6.28	sparse forest canopy	6.17			
4	306937.5	4161218	0.05	0.03	0.21	0.31	0.09	bare soil	0.14	2.24	3.70	4.59
5	307000	4161280	0.26	0.23	0.36	0.4	0.8	bare soil	0.41			
6	307125	4161405	7.31	6.71	7.11	6.9	6.04	dense forest canopy	6.81			
7	307312.5	4161530	6.34	6.86	6.31	6.66	6.39	moderate forest canopy	6.51			
1	306562.5	4159843	0.9	0.53	4.35	5.09	4.23	peach field	3.02			
2	306750	4160030	1.51	1.4	1.33	1.6	1.42	Crop field	1.45			
3	306875	4160155	1.38	1.29	1.63	1.37	1.44	Crop field	1.42			
4	306937.5	4160217	1.12	1.11	1.18	1.11	1.17	Crop field	1.14	1.31	1.42	2.43
5	307000	4160280	0.06	1.88	1.59	1.72	1.65	strawfield	1.38			
6	307125	4160405	2.12	1.64	1.87	1.43	1.59	Crop field	1.73			
7	307312.5	4160593	7.01	7.46	6.68	6.88	6.36	high forest canopy	6.88			

VITA

Graduate School
Southern Illinois University

Kushendra Narayan Shah
knshah@siu.edu

Kathmandu University
Bachelor of Science, Environmental Science, Nov 2008

Thesis Title:
Multi-scale Mapping and Accuracy Assessment of Leaf Area Index for Vegetation Study in Southern Illinois.

Major Professor: Dr. Guangxing Wang